POLITECNICO DI TORINO
Repository ISTITUZIONALE

A comparative study of two SOFC based cogeneration systems fed by municipal solid waste by means of either the gasifier or digester

Original
A comparative study of two SOFC based cogeneration systems fed by municipal solid waste by means of either the gasifier or digester / Yari, M., Mehr, A.S., Mahmoudi, S.M.S., Santarelli, M.. - In: ENERGY. - ISSN 0360-5442. - 114:(2016), pp. 586-602. [10.1016/j.energy.2016.08.035]

Availability:
This version is available at: 11583/2648246 since: 2016-09-12T16:07:51Z

Publisher:
Elsevier Ltd

Published
DOI:10.1016/j.energy.2016.08.035

Terms of use:

This article is made available under terms and conditions as specified in the corresponding bibliographic description in the repository

Publisher copyright

(Article begins on next page)

16 October 2026

A comparative study of two SOFC based cogeneration systems fed by municipal solid waste by means of either the gasifier or digester

M. Yari[1], A. S. Mehr[1,*], SMS Mahmoudi[1] and M. Santarelli[2]

1. Faculty of Mechanical Engineering. University of Tabriz, Tabriz, Iran
2. Department of Energy, Politecnico di Torino, C.so Duca degli Abruzzi 24, 10129, Turin, Italy

Abstract

Two new cogeneration systems (producing power and heating) based on solid oxide fuel cell fed by either the syngas or biogas is proposed. The performance of systems is analyzed and compared with each other from the thermodynamic and economic viewpoints. Applying the conservation of mass and energy as well as the exergy and cost balance for each system component and using the engineering equation solver software, the systems are modeled. Through a parametric study, effect of some key variables such as the current density and the stack temperature difference on the systems' performance is investigated. It is found that for power generation, digester based solid oxide fuel cell shows better performance of first law efficiency (40.14% vs 20.31%); however considering the combined power and heating system, the difference becomes less (51.05% vs 58.75%). In addition, it is found that the digester based SOFC is more cost-efficient and has 54% less unit product cost compared to that of the gasifier based system. Results of exergy analysis reveal that the air heat exchangers and the gasifier are the two major sources of irreversibility in the systems. Finally, a method of choosing the systems based on the need and the cost is presented.

Keywords: *SOFC, Biogas, Syngas, Gasifier, Anaerobic Digester, Exergoeconomic, comparative study*

***Corresponding author e-mail:** a.s.mehr@tabrizu.ac.ir (Ali Saberi Mehr)

Tel.: +98 41 33392487; fax: +98 41 33354153.

Nomenclature

AD	Anaerobic digester
AHX	Air heat exchanger
D-SOFC	Digester coupled SOFC
G-SOFC	Gasifier coupled SOFC
SOFC	Solid oxide fuel cell
HRSG	Heat recovery steam generator
EES	Engineering Equation Solver
FHX	Fuel heat exchanger
FuelB	Fuel blower
AirB	Air blower
P	pump
K	equilibrium constant
ΔG	Change in Gibbs function
S	entropy
h	enthalpy
$\dot{W}$	Power
$\dot{Q}$	Heating load

Subscript and abbreviations

0	dead state
1,2,3,…	state points

Greek Symbols

η_{th}	thermal efficiency
η_{II}	exergy efficiency
η_{I}	energy efficiency
η_{is}	isentropic efficiency

1. Introduction

Since the world's energy consumption is forecast to rise remarkably during the next two decades, no one can deny the importance of renewable energy sources. In addition, continued demand for fossil fuels means the world will not be able to reduce greenhouse gases in the atmosphere. In this regard, implementing the power plants utilizing the renewable energy sources such as geothermal, solar, biofuel, biomass and so on, is supposed to be of governments' and researchers' interest.

Recent developments in solid oxide fuel cell (SOFC) technology have increased interest in the application toward electricity generation particularly the distributed one. In addition to the advantages of SOFC system over conventional power generation methods, heat from SOFC exhaust can be recovered for combined heat and power (CHP) operations to improve the overall system efficiency.

Undoubtedly, the hydrogen is the genuine fuel for the stack; however, considering its cost and availability, using the natural gas could be more viable, practical and economical in addition to the reforming process of the fuel. Nevertheless, feeding the SOFC with fuels such as biogas, biofuels, syngas and alcohols has become of great interest as they could be suitable alternatives for the natural gas. There are numerous solid waste gasification facilities operating or under construction around the world. Gasification has several advantages over traditional combustion processes for municipal solid waste (MSW) treatment. It takes place in a low oxygen environment that limits the formation of dioxins and of large quantities of SO_x and NO_x. Furthermore, it requires just a fraction of the stoichiometric amount of oxygen necessary for combustion (partial oxidation). As a result, the volume of process gas is low, requiring smaller and less expensive gas cleaning equipment. The lower gas volume also means higher partial

pressure of contaminants in the off-gas, which favors more complete adsorption and particulate capture. Finally, gasification generates a fuel gas that can be integrated with combined cycle turbines, reciprocating engines and, potentially, with fuel cells converting fuel energy to electricity more efficiently than conventional steam boilers[1,2]. Renewability and less CO_2 emission are the greatest advantages of commonly used biomass fuels such as paper, wood, waste straw, saw dust, paddy husk, MSW, etc. [3–6].Three processes are usually involved in thermochemical conversion of biomass into usable fuels for power plants: combustion, gasification and pyrolysis [7,8]. The gasification process proves to be an efficient technique as it transforms biomass into easily usable fuels to be used for electricity generation [9–11]. There are different types of gasifiers based on the types of moving fluid and solid inside[12]. From the availability view point however, 75% percent of the gasifiers are downdraft, 20% is circulating fluidized bed, 2.5% updraft and 2.5% the other kinds [13].

A 200kW SOFC combined heat and power system has been developed by Omosun et al. [14] to evaluate the system efficiency and its cost analysis. Two different options were investigated; one of them involved cold gas cleaning and the other used hot gas cleaning. The results revealed that system efficiency for the hot process is higher than that for the cold process due to the better heat management in the cleaning process and higher gasification temperature. Despite the capital cost for the hot process is marginally higher, income earned from selling the extra heat produced may justify the additional cost. Singh et al. [15] analyzed the carbon deposition in a solid oxide fuel cell (SOFC) fueled by a biomass. It is reported that carbon deposition decreased to zero as the operating conditions were varied to get a fuel mixture with higher water content (about 15%). The conjunction of biomass gasification with solid oxide fuel cells is investigated by Athanasiou et al. [16] and the results showed that the electrical efficiency of the integrated gasification-

SOFC-steam turbine is about 68% higher than that for the conventional gasification-steam turbine system. A direct internal reforming-SOFC (IR-SOFC) operating with syngas was modeled thermodynamically by Colpan et al [17]. The results showed that recirculation ratio does not have a significant effect for low current density conditions. However, at higher current densities, increasing the recirculation ratio decreases the output power and electrical efficiency of the cell. Jang et al. [18] studied a direct power generation from waste coffee grounds in a biomass fed fuel cell. Results show that biomass type has crucial effect on cell performance. They used waste coffee ground (WCG) as biomass with the benefit of not needing any pre-reformer in the system. It is reported that at cell operating temperature of 900°C the system shows maximum power density twice than that of the carbon black. Pieratti et al. [19] investigated experimentally and theoretically the syngas suitability for solid oxide fuel cell applications. Considering environmental aspects of biomass combustion, steam gasification is used to produce syngas. Experimental data is used to generate and calibrate a 2D theoretical equilibrium model. It is found that the thermodynamic approach is a simple engineering useful tool to obtain reliable results of the gasification model. It is declared that considering the syngas composition and energy content, the obtained syngas is a suitable fuel for fuel cells. Nevertheless, the gas cleaning is still one of the main critical issues. In particular the tar and the H_2S in the gas can rapidly decrease the life of the fuel cells. A new small cogeneration system consisting of a fluidized bed gasifier, coupled to a SOFC and a micro gas turbine is proposed by Di Carlo et al. [20]. Results disclosed that the best case occurs with a temperature of the cathode gas of 800 ^{o}C and moisture of 10%, in this case the fuel utilization could be set equal to 0.79 and the electrical efficiency of the overall system is 48%. Focusing on the anode gas recycling, Lorenzo and Fragiacomo [21] analyzed the performance of syngas fed SOFC power plant from

98 the viewpoint of thermodynamics. It is reported that there is an optimum value for anode gas
99 recycle ratio in which the thermal efficiency is maximized. An integrated SOFC and biomass
100 (wood) gasification system using air, enriched air, and steam as gasification agent is investigated
101 by Jia et al. [22]. It is found that when using air or oxygen-enriched air as gasification agent, the
102 gasifier reactor caused the greatest exergy destruction while for steam gasification power
103 systems the largest exergy destruction lies in air heat exchanger. Also, for the efficient CHP case
104 the exergy efficiency is calculated to be 36%. In another work, Jia et al. [23] studied the effects
105 of various parameters such as moisture content in biomass, equivalence ratio and mass flow rate
106 of dry biomass on the overall performance of SOFC based CHP system. It is reported that char in
107 the biomass tends to be converted with decreasing of moisture content and increasing of
108 equivalence ratio due to higher temperature in reduction zone of gasifier. Kartha et al. [24]
109 studied a small-scale biomass fuel cell/gas turbine power systems for rural areas. A downdraft
110 gasifier is used to produce syngas because it is reported to be commercialized and simple in
111 design which has very little amounts of tar (the excessive production of which needs a separate
112 reactor for tar removal and dissipates amounts of flue gas energy) and has simple method of gas
113 cleaning. Also, the efficiency of the studied SOFC-GT was found to be 43.4%. Federico
114 Ghirardo et al. [25] studied heat recovery options for fuel cells. It is found that about 181 kW of
115 heat can be recovered in an ORC to produce 35 kW of electricity. The overall efficiency
116 increases from 44% to 49% when the recovery system is used and the cost of energy drops from
117 25 c$/kWh (isolated SOFC system) to 22 c$/kWh.

118 Even though continued progress has been made with other alternative treatment technologies
119 (gasification, pyrolysis, plasma, biological drying, etc.), these technologies have by far not seen
120 the same widespread implementation that anaerobic digestion has been able to achieve. In

Europe alone, 244 installations dealing with the organic fraction of municipal solid waste as a significant portion of the feedstock have been constructed or are permitted to be constructed. Feeding SOFCs by biogas is investigated by researchers in the recent years. The performance of biogas-fed solid oxide fuel cell system utilizing different reforming agents (steam, air and combined air/steam) was investigated by Piroonlerkgul et al. [26]. It is observed that for the steam-fed SOFC, there is an optimal amount of steam which provides a maximum power density. However, for the air-fed SOFC system, the power density always decreases with the increase of amount of air due to the dilution effect of nitrogen in air. Three configurations of biogas fed solid oxide fuel cell micro-combined heat and power (micro-CHP) systems are studied with a particular emphasis on the application for single-family detached dwellings by Farhad et al. [27]. Tjaden et al. [28] investigated a small scale biogas-SOFC plant in 2014. Results show that the maximum electrical efficiency is calculated 56.55% which is 15% higher than that of the combustion engines fueled by biogas. Also, the advantages and disadvantages of different reforming process such as steam reforming and auto thermal reforming are reported. The results revealed that the cell design voltage is higher than the cell voltage at which the minimum number of cells is obtained for the SOFC stack. Also, the maximum electrical efficiency of 42.7% is obtained for one of the configurations. Producing biogas from biomass and then feeding either the SOFC or internal combustion engine is studied by Santarelli et al. [29]. Optimization results revealed that produced electrical energy for the SOFC is higher than that for the internal combustion engine where the consumed thermal energy is the same for both systems. Papurello et al. [30] studied the performance of a biogas-fed SOFC power plant experimentally. A 500 W_{el} SOFC stack was installed at a biomass digester pilot plant and was fed with real biogas for more than 400 hours, after which a stable voltage was achieved under

partial oxidation reforming conditions. The fuel utilization was approximately 55% and the electrical efficiency was close to 34%. The biogas which is obtained from organic waste collection from local municipal areas via digester consists of methane and carbon dioxide concentrations ranging from 60-70% and 30-40% vol., respectively. Trendewicz and Braun [31] analyzed a biogas-fueled solid oxide fuel cell (SOFC) system for producing heat and power from the view point of techno-economic. They estimated that the baseline cost of electricity for the small, the medium, and the large plants is 0.079 $/kWh, 0.058 $/kWh and 0.05 $/kWh, respectively. Gandiglio et al. [32] proposed a model to analyze the integration of waste water treatment (WWT) biogas and solid oxide fuel cell considering both the internal and external reforming. The influence of fuel utilization, internal reforming, biogas composition and steam-to-carbon ratio on both the SOFC and overall plant performance is investigated. It is observed that an increase in the methane concentration of biogas would increase the electrical efficiency of the plant slightly. Siefert and Litster [33] investigated the performance of a biogas-fed SOFC from the viewpoint of economics. Their interesting result may be the one revealing that the anaerobic digestion-SOFC system is significantly more economic than the systems in which the biogas is sent to internal combustion engines or micro gas turbines. An exergoeconomic analysis of biogas-fed SOFC power systems focusing on the (anode/cathode) gas recycling investigated by Mehr et al. [34]. It is reported that, the solid oxide fuel cell system with anode and cathode recycling is superior to the other configurations and its efficiency is calculated as 46.09% being 6.81% higher than that of the simple solid oxide fuel cell fed by natural gas. The unit product cost of the solid oxide fuel cell system with anode and cathode gas recycling is calculated as 19.07$/GJ which is about 35% lower than the corresponding value for the simple natural gas fed solid oxide fuel cell system.

As discussed above, there are two common ways to produce gas from the biomass, using gasifier or digester. In the present work, a downdraft gasifier and a thermophilic digester are used to produce syngas and biogas from the municipal solid waste, respectively. The produced gases are supposed to drive the SOFC system to produce power. As the compositions of biogas and syngas are quite different, and also the exhaust of SOFC is hot enough, the CHP system would be an interesting choice to utilize the hot exhaust of SOFC stack to produce heating. Also, it would be interesting to reveal which system is more efficient and more economical with the almost same working conditions. Modeling of the systems is performed in EES software and the performance of systems is compared with each other from the thermodynamics and thermo-economics viewpoints.

2. System description and assumptions

2.1 Systems configuration

Schematic diagram of the proposed cogeneration system based on the digester unit system is illustrated in Fig.1a. The system consists of a biogas production unit, a SOFC with anode recycling and heat recovery steam generator (HRSG). Biomass is sent to the digester at environmental conditions and as the digester is considered thermophilic one the temperature of biogas exiting the digester will be higher than environment temperature. Then the biogas is sent to the cleanup unit, in which H_2S is coldly removed and then the clean biogas is sent to the blower. The biogas and air are preheated through the fuel heat exchanger and air heat exchanger, respectively, after being pressurized with the help of fuel and air blowers (the pressure is just to make a flow of fuel and air and compensate the pressure drops within the system). The heated air is sent to the cathode of the stack. On the other hand, the biogas is sent to the anode after mixing

with the recycling of anode stream (state15). The mixed stream experiences the internal reforming process which brings hydrogen-rich products participating in the electrochemical reaction inside the fuel cell stack. An inverter is used to convert the DC power generated by the stack into grid quality electricity. The electrochemical reaction generates thermal energy a part of which is used to deliver the required heat of the internal reforming reaction, another part is employed to heat up the cell products and residual reactants, and the remaining small amount is transferred to the environment as a heat loss (in the present modeling heat loss is neglected). After the finishing of electrochemical reaction in the SOFC stack, the excess air out of the cathode and the unreacted fuel out of the anode combust completely in an after-burner to generate the combustion gas under high temperature. The exhaust gas from the afterburner is sequentially used to preheat the fuel and air, respectively. The exhaust (state 15) is still hot enough to be utilized to produce hot steam. Therefore, a HRSG unit is considered to be coupled with SOFC system. For the maintenance of the digester temperature in the thermophiles condition, the produce hot water can be used to compensate the heat demand of digester. Fig. 1b depicts the use of syngas produced in the gasification process to produce power and heating by means of SOFC power plant and HRSG unit. The description of the process for the system is almost the same as described for the Fig. 1a. The air from environment is brought to the gasifier along with the biomass in the atmospheric pressure. The equilibrium model is presumed in modeling the gasifier. The equilibrium modeling assumes that all the reactions are in thermodynamic equilibrium and that the pyrolysis product (gas) which is product of interest burns and achieves equilibrium in the reduction zone before leaving the downdraft gasifier. Meanwhile, the high temperature syngas produced in gasifier first used to preheat the air before sending it to the mixer to be mixed with anode gas recycle.

2.2 Assumptions

Some meaningful assumptions are considered for the systems modeling as listed below [35,36];

- The atmospheric air is composed of 79% N_2 and 21% O_2, on a volume basis.
- Gasification temperature is assumed to be 1073 K and the syngas is in thermodynamic equilibrium
- A thermophilic digester is used in the modeling
- Fan work in the digester is negligible
- All gases are treated as ideal gases and gas leakage from the components and the connecting pipes is negligible.
- The analysis is carried out under thermodynamic equilibrium and steady state conditions.
- Changes in kinetic and potential energies are neglected.
- Temperatures at channel inlets are the same and, similarly, temperatures at the channel exits are the same.
- The fuel cell is insulated perfectly so that there is no heat interaction with the environment
- Contact resistances are negligible.
- Unreacted gases are assumed to be fully oxidized in the afterburner. [37]

The input data for systems' simulation are listed in Table 1.

3. Energy analysis

3.1 Gasifier modeling

The equilibrium model presumed in gasifier modeling assumes that all the reactions are in thermodynamic equilibrium and that the pyrolysis product burns and achieves equilibrium in the

234 reduction zone before leaving the downdraft gasifier [36]. The reactions in the reduction zone
235 are as stated in the literature [36,38,39].

$$CH_aO_bN_c + wH_2O + m\left(O_2 + 3.76N_2\right) \rightarrow n_1H_2 + n_2CO + n_3CO_2 + n_4H_2O + n_5CH_4 + n_6N_2 \quad (1)$$

236 For a biomass, the global gasification reaction is as follows [40]:

237 The equilibrium constants for methane formation reaction and for the water-gas reaction (shift

$$K_1 = \frac{n_5}{n_1^2}\left(\frac{P/P_{ref}}{n_{tot}}\right)^{-1} \quad (2)$$

$$K_2 = \frac{n_1 n_3}{n_2 n_4}\left(\frac{P/P_{ref}}{n_{tot}}\right)^{0} \quad (3)$$

238 reaction) are given by Eqs. 2 and 3, respectively [38]:

239 where n_1 to n_5 are the number of moles in the gasification products in eq. 1. and K_1 and K_2 are
240 the equilibrium constants which can be related to the change in the Gibbs function as follows
241 [38]:

$$\frac{-\Delta G_1^0}{\bar{R}T_g} = ln\, K_1 \quad (4)$$

242

$$\frac{-\Delta G_2^0}{\bar{R}T_g} = ln\, K_2 \tag{5}$$

Where $-\Delta G_1^0$ and $-\Delta G_2^0$ are the change in the Gibbs free function of methane formation equation and shift reaction respectively[36].

In Eq. 1, $CH_aO_bN_c$ denotes the biomass, *w* is the biomass moisture content and *m* is the kmol of oxygen per kmol of biomass. The parameter *m* is actually the air fuel ratio and can be determined if the gasification temperature is known (or vice versa). The coefficients n_1 to n_6 are determined through applying the mass balance for *H*, *C*, *O* and *N*. Based on the ultimate analysis of the MSW as given in Table 2.

The moisture content per mole of biomass can be expressed in terms of mass based moisture content (MC) as follows [36]:

$$w = \frac{M_{biomass}\, MC}{18\,(1-MC)} \tag{6}$$

where,

MC = (mass of water/mass of wet biomass)$\times$ 100

Assuming an adiabatic gasification at a temperature of 1073 K, the energy balance equation, as indicated below, is solved to find the air fuel ratio.

$$\begin{aligned}\bar{h}_{f-MSW}^0 + w\,(\bar{h}_{f-H_2O}^0) &= n_1\left(\bar{h}_{f-H\,2}^0 + \Delta\bar{h}_{H_2}\right) + n_2\left(\bar{h}_{f-CO}^0 + \Delta\bar{h}_{CO}\right) \\ &+ n_3\left(\bar{h}_{f-CO\,2}^0 + \Delta\bar{h}_{CO\,2}\right) + n_4\left(\bar{h}_{f-H\,2O}^0 + \Delta\bar{h}_{H\,2O}\right) + n_5\left(\bar{h}_{f-Ch\,4}^0 + \Delta\bar{h}_{Ch\,4}\right) + n_6\left(\bar{h}_{f-N\,2}^0 + \Delta\bar{h}_{N\,2}\right)\end{aligned} \tag{7}$$

In order to validate the gasification model, the experimental and theoretical data reported in

257 the literature are used for gasification temperature of 1100K and moisture content of 16%. The
258 comparison is shown in Table 3. Referring to Table 3, the sum of hydrogen and carbon
259 monoxide content percentages predicted by the present model is 36.43%, which agrees with the
260 experimental data (35.4%) reported by Jayeh [41]. It is found that the obtained results for the
261 present model agree well with those reported by Jarungthammachote [42] as well.

262 In order to validate the simulation results of SOFC, the available experimental data reported
263 by Tao et al. [43] is used. Table 4 compares the cell voltage and power density obtained in the
264 present model developed by the authors and those reported by Tao et al. [43]. The comparison
265 shows a good agreement between them.

266 3.2 Digester modeling

267 In modeling of digester, a thermophilic anaerobic digester with a temperature of 55°C is used.
268 Note that, it is necessary that temperature fluctuations do not occur in the digester to maintain the
269 microbial activity.

270 With knowledge of chemical composition of MSW outlined as ultimate analysis in Table 2
271 the biogas composition can be predicted following the method proposed by Baswell and Hatfield
272 [44]. The global reaction occurring in the digester to produce biogas is:

$$C_nH_aO_b + wH_2O \rightarrow n_1CO_2 + n_2CH_4 \quad (8)$$

273 In the present work, it is assumed that 0.95 of the OFMSW is volatile. A well designed
274 digester aims to destruct at minimum 0.7 of the volatile solid. Following the procedure presented
275 by Murphy[45] the methane and carbon dioxide mass is found. Knowing that the number of
276 molecules in a unit volume under standard conditions is the same for all gases (This volume is
277 22.412m^3/kg) one may find that the 58% of the biogas is methane and 42% of biogas is carbon

dioxide in volume.

3.3 SOFC with anode recycle model

Energy analysis and molar balance for the SOFC with anode and cathode recycle is used in the present work. [46][46]The biogas is converted into a hydrogen-rich synthesis gas inside the fuel cell by making use of internal reforming and shifting reactions [35]. Also syngas (with hydrogen gas) which does not need any reforming and less methane and carbon monoxide gas is reformed inside the SOFC with the same processes as for biogas. The use of an internal reformer also reduces the dependence of the fuel cell on a cooling system. The chemical reactions in the cells are as follows; [47]

$$CH_4 + H_2O \rightarrow CO + 3H_2 \quad \text{(Reforming)} \tag{9}$$

$$CO + H_2O \rightarrow CO_2 + H_2 \quad \text{(Shifting)} \tag{10}$$

Equation 9 is reforming reaction and equation 10 is shifting reaction, carbon monoxide in the reforming reaction, reacts with the water which is brought to the SOFC by means of either recycling or externals means such as pump, to produce hydrogen. Hydrogen from shifting

$$H_2 + \frac{1}{2}O_2 \rightarrow H_2O \quad \text{(overall electrochemical reaction)} \tag{11}$$

reaction is used in the electrochemical reaction as below:

The molar conversion rates for reforming, shifting and electrochemical reactions are considered to be x_r, y_r, and z_r, respectively. Therefore, rates of consumption and production of the components can be achieved by the following model:

$$x_r \rightarrow [CH_4 + H_2O \rightarrow CO + 3H_2] \quad \text{(Reforming)} \tag{12}$$

$$y_r \rightarrow [CO + H_2O \leftrightarrow CO_2 + H_2] \quad \text{(shifting)} \tag{13}$$

$$z_r \rightarrow \left[H_2 + \frac{1}{2} O_2 \rightarrow H_2O \right] \quad \text{(Overall electrochemical reaction)} \tag{14}$$

294 z_r, could be found with the help of current density, Faraday constant, cell number, and active

$$z_r = \frac{j\, N_{FC}\, A_a}{2F} \tag{15}$$

295 surface area, as followed by equation (16)

296 Applying mass balance equations along with considering equations 13-16 for the mixing units
297 and the whole SOFC model the flowing gas compositions may be achieved. In order to solve the
298 system of equations, 3 more equations are needed to complete the system of the equations.
299 Looking again in the equilibrium reactions of shifting and reforming, the equilibrium constants

$$\ln K_s = -\frac{\Delta \bar{g}_s^o}{\bar{R} T_{FC,e}} = \ln \left[\frac{(\dot{n}_{CO_2,11} + y_r)\left(\dot{n}_{H_2,11} + 3x_r + y_r - z_r\right)}{\left(\dot{n}_{CO,11} + x_r - y_r\right)\left(\dot{n}_{H_2O,11} - x_r - y_r + z_r\right)} \right] \tag{16}$$

$$\ln K_R = -\frac{\Delta \bar{g}_R^o}{\bar{R} T_{FC,e}} = \ln \left[\frac{(\dot{n}_{CO,11} + x_r - y_r)\left(\dot{n}_{H_2,11} + 3x_r + y_r - z_r\right)^3}{\left(\dot{n}_{CH_4,11} + x_r\right)\left(\dot{n}_{H_2O,11} - x_r - y_r + z_r\right) \times \dot{n}_{12}^2} \left(\frac{P_{12}}{P_{ref}} \right)^2 \right] \tag{17}$$

300 can be written as follows respectively:

301 Where, $\bar{R}$ and $T_{FC,e}$ are the universal gas constant and the temperature at the exit of the
302 SOFC, respectively. Also, $\Delta \bar{g}^o$ is the change in the Gibbs free function of shifting and reforming

reactions[35].

The last equation needed for solving the system equations is obtained using the energy balance for the whole stack. Neglecting the heat loss from the stack, the energy balance can be

$$\dot{W}_{FC,stack} = \sum_{k} \dot{n}_{k,12} \bar{h}_{k,12} + \sum_{L} \dot{n}_{L,4} \bar{h}_{L,4} - \sum_{m} \dot{n}_{m,11} \bar{h}_{m,11} - \sum_{n} \dot{n}_{n,3} \bar{h}_{n,3} \quad (18)$$

written as follows;

Where, *k*, *L*, *m* and *n* are the corresponding gas compositions in each states (e.g. gas composition at state 12 (*L*) is CO_2, CO, H_2O, CH_4, N_2 and H_2)). On the other hand, the work rate

$$\dot{W}_{FC,stack} = N_{FC}\, j\, A_a V_c \quad (19)$$

produced by the SOFC stack $\dot{W}_{FC,stack}$ can be expressed as:

$$V_c = V_N - V_{loss} \quad (20)$$

Where cell voltage is defined as:

Here, V_N is the Nernst voltage and V_{loss} the voltage loss, which is the sum of three separate voltage losses; Ohmic, Activation and Concentration losses:

$$V_{loss} = V_{ohm} + V_{act} + V_{conc} \quad (21)$$

Looking again in the comprehensive analysis of the cell voltage and voltage losses it is found that voltages strongly depend on molar fractions, pressures, electrolyte types and cell operating

temperature that need to be verified very precisely. For the sake of brevity detailed voltage modeling used in the present work has been presented in Appendix A.

3.4 Heat recovery steam generator analysis

One of the determinant parts of the proposed systems is HRSG, which affects the final system specifications and has crucial effect on determining whether to choose gasifier or digester. Gas flow from the AHX is hot enough that can be utilized to generate saturated steam in HRSG. As shown in Fig. 1a and Fig. 1b the HRSG involves economizer (Eco) and evaporator (Eva) parts. Water is pressurized by a pump (P) to meet the required steam pressure for the HRSG.

Applying the energy balance as well as the pinch point temperature difference for the whole HRSG system the mass flow rate of steam and temperature of exhaust can be determined. Energy balance for the economizer and the evaporator parts are as follows:

$$\sum_j n_j \left(\bar{h}_{f_j}^0 + \Delta\bar{h}\right)_{exhaust\ gas,in} + n_{water,in}\,\bar{h}_{water,in} = \sum_j n_j \left(\bar{h}_{f_j}^0 + \Delta\bar{h}\right)_{exhaust\ gas,out} + n_{water,out}\,\bar{h}_{water,out} \quad (22)$$

Where the amount of heat used for generating hot steam is defined as;

$$\dot{Q}_{Heating} = \dot{m}_{product\ gas}(h_{15} - h_{17}) \quad (23)$$

3.5. First law efficiency for proposed system

Finally with regarding the above mentioned analysis, the first law efficiency for the power generation (electrical efficiency) mode and CHP mode could be defined as follows respectively:

$$\eta_{\mathrm{I,P}} = \frac{\dot{W}_{FC,stack,ac} - \dot{W}_{FC} - \dot{W}_{AC} - \dot{W}_{pump}}{\dot{m}_{biomass} LHV_{biomass}} \quad (24)$$

$$\eta_{\mathrm{I,CHP}} = \frac{\dot{W}_{FC,stack,ac} - \dot{W}_{FC} - \dot{W}_{AC} - \dot{W}_{pump} + \dot{Q}_{Heating}}{\dot{m}_{biomass} LHV_{biomass}} \quad (25)$$

330 Where $\dot{W}_{FC}, \dot{W}_{AC}$ *and* $\dot{W}_p$ is the amount of fuel compressor power and air compressor power
331 required to blow the fuel and air to the SOFC and pump required power respectively.

332 4. Exergy analysis

333 An effective use of energy can be assessed by means of exergy analysis for energy converting
334 systems. Exergy can be divided into four parts: physical, chemical, kinetic and potential
335 exergies. For the processes involved in this paper, the latter two are neglected since the changes
336 in elevation and velocity are negligible [48,49]. Thus, the specific exergy of any stream is
337 expressed as

$$e = e_{ph} + e_{ch} \quad (26)$$

338 where the physical exergy is defined as [48] :

$$e_{ph,i} = h_i - h_0 - T_0 \left(s_i - s_0 \right) \quad (27)$$

339 The specific chemical exergy of a solid biomass fuel can be expressed as follows [36]:

$$e^{ch}_{biomass} = \beta \, LHV_{biomass} \quad (28)$$

340 where the factor β in Eq. 28 denotes the ratio of the chemical exergy to the lower heating value
341 (LHV) for the organic fraction of the biomass. A statistical correlation for the β is provided by
342 Szargut and Styrylska [36]:

$$\beta = \frac{1.044 + 0.16\frac{z_H}{z_c} - 0.34493\frac{z_o}{z_c}\left(1 + 0.0531\frac{z_H}{z_c}\right)}{1 - 0.4142\frac{z_o}{z_c}} \quad (29)$$

where z_H, z_c, z_o are the weight fractions of the hydrogen, carbon and oxygen in the biomass, respectively. The chemical exergy of an ideal gas mixture can be expressed as [48]:

$$e_i^{ch} = \sum_i x_i e_{0,i}^{ch} + \bar{R}T_0 \sum_i x_i ln x_i \quad (30)$$

where x_i is the mole fraction of i_{th} component and $e_{0,i}^{ch}$ is the standard chemical exergy of that component [38]. The exergy balance for a system component is expressed as:

$$\sum \dot{E}_{In} = \sum \dot{E}_{out} + \dot{E}_D \quad (31)$$

With the aid of eq. 31 one may find the exergy destruction in system components in order to define the most probable candidate of optimizing for higher efficiency.

Finally, exergy analysis can be completed by defining the efficiency of second law for the power generation (electrical efficiency) mode and CHP mode as follows:

$$\eta_{\mathrm{II,P}} = \frac{\dot{W}_{FC,stack,ac} - \dot{W}_{FC} - \dot{W}_{AC} - \dot{W}_{pump}}{\dot{E}_{in}} \quad (32)$$

$$\eta_{\mathrm{II,CHP}} = \frac{\dot{W}_{FC,stack,ac} - \dot{W}_{FC} - \dot{W}_{AC} - \dot{W}_{pump} + (\dot{E}_{22} - \dot{E}_{20})}{\dot{E}_{in}} \quad (33)$$

where $\dot{E}_{in}$ is the rate of input exergy and can be defined as below for gasifier coupled SOFC and digester coupled SOFC respectively:

$$\dot{E}_{in} = e_{biomass}^{ch} + w\, e_{water}^{ch} + 4.76\, m\, e_{air}^{ch} + \dot{E}_6 + \dot{E}_{19} \quad (34)$$

$$\dot{E}_{in} = e^{ch}_{biomass} + w\, e^{ch}_{water} + \dot{E}_{19} \quad (35)$$

5. Economic analysis

5.1. Methodology

It seems that investigating the performance of a system without looking at its product cost will not be accomplished. Integration of economic point of view with thermodynamic seems to be appealing. Exergoeconomic method firstly introduced by Tsatsaronis et al. [50] gets the interest of researchers who use the method to analyze the thermodynamic systems from the viewpoint of economic. The purpose of exergoeconomic analysis for a system is to disclose the cost formation processes and calculate the cost per unit exergy of product streams. To calculate the cost of each unit exergy stream, the cost balance equation along with the required auxiliary equations are applied to each component of the systems. For a system component receiving thermal energy and generating power, the cost balance is written as:

$$\sum \dot{C}_{out,k} + \dot{C}_{w,k} = \sum \dot{C}_{in,k} + \dot{C}_{q,k} + \dot{Z}_{k,PY} \quad (36)$$

$$\dot{C} = c\ \dot{Ex} \quad (37)$$

Where, c is the cost per exergy unit and $\dot{Ex}$ is the total exergy rate.

In equation (36), $\dot{Z}_{k,PY}$ is the appropriate charge due to capital investment and operating and maintenance expenses for each component in a reference year. Note that, the cost of the system components which are available in an original year is converted from that original time to a same reference year (year 2013 for present work) with the help of Chemical Engineering Plant Cost Index (CEPEI).

$$\dot{Z}_k^o = \dot{Z}_k^{o,CI} + \dot{Z}_k^{o,OM} \tag{38}$$

370 Cost at reference year=Original cost$\times\frac{\text{Cost index for the reference year}}{\text{Cost index for the original year}}$

371 Or

$$\dot{Z}_{k,PY} = \dot{Z}_k^o \frac{CI_{k,PY}}{CI^o} \tag{39}$$

372

373 The term $\dot{Z}_k^o \dot{z}_k$ in Eq. (38) can be calculated as [48]:

$$\dot{Z}_k^o = \frac{Z_k \; CRF \; \varphi}{N} \tag{40}$$

374 Where φ is the maintenance factor, *N* is the number of system operating hours in a year and
375 *CRF* is the Capital Recovery Factor, which can be expressed as [51]:

$$CRF = \frac{i_r \left(1+i_r\right)^n}{\left(1+i_r\right)^n - 1} \tag{41}$$

376 Here, i_r is the interest rate and *n* is the system life. The input data used in economic
377 evaluations along with the cost and auxiliary equations for each component of the systems is
378 gathered in Table 5.

379 5.2 Cost evaluation

380 To obtain the cost of all unit exergy streams, the linear system of equations is solved
381 assuming that the cost of unit exergies associated with the input fuel is an input.

382 The exergoeconomic evaluation of the systems is carried out using the thermoeconomic

383 variables, namely, the unit cost of the fuel ($c_{F,k}$), the unit cost of the product ($c_{P,k}$), the cost rate of
384 exergy destruction ($\dot{C}_{D,k}$), the cost rate of exergy loss ($\dot{C}_{L,k}$) and the thermoeconomic factor (f_k).
385 These parameters are calculated using the following relations [48]:

386 # 6. Results and discussions

387 The effect of decision parameters such as the current density, the temperature difference of
388 SOFC stack on efficiencies of power generating system and CHP system along with net power
389 output, heating capacity and unit product cost of the systems is investigated. Nominal values of
390 current density, where maximum power is achieved, are found to be 0.6 mA/cm^2 and 0.2
391 mA/cm^2 for the D-SOFC and G-SOFC systems respectively.

392 Fig. 2 shows the effect of current density on the first and second law efficiencies of the power
393 generating system. Referring to Fig. 2, the current density range is lower for G-SOFC system
394 because of N_2 presence in the gasifier exit, which causes partial pressure of components in stack
395 exit to become less than the D-SOFC system and it affects the cell voltage due to decrease in J_{0a}.
396 Looking again in Fig 2, for constant value of fuel utilization factor both first and second law
397 efficiencies tend to decrease with increasing current density. With increasing 0.6 A/cm^2 in
398 current density for the D-SOFC system, first and second law efficiencies tend to decrease by an
399 almost 40%. While the reduction is about 30% for the G-SOFC system (with a possible increase
400 of 0.2 A/cm^2).

401 Fig. 3a shows the effect of current density on the first and second law efficiencies of the CHP
402 system. The results show that the first law efficiency for the G-SOFC system is in the range of
403 50%- 74% while the efficiency for the D-SOFC system is obtained in the range of 35%-84%.
404 The great difference between the first and second law efficiency values for G-SOFC system is

405 due to the exergy rate within the HRSG system (exergy related to heating).

406 Fig. 3b shows the effect of current density on both the net power output and heating capacity.
407 First important point is that, the net power output is maximized for specific values of current
408 density for both the D-SOFC and G-SOFC systems. The optimum current density value for G-
409 SOFC system is found to be 0.199 A/cm^2 and the corresponding net power output is calculated
410 46.98 kW. For the D-SOFC system the optimum current density and net power values are 0.64
411 A/cm^2 and 159.7 kW, respectively. In addition, it is observed that an increase in the current
412 density increases the heating capacity with an almost same trend of power. At the optimum
413 working points (where the net power output is maximized) the heating capacity values are
414 88.3kW and 43.31kW for the G-SOFC and D-SOFC systems, respectively. Another important
415 aspect of Fig 3b is that although the net power output is higher for the digester based system, the
416 heating capacity is higher for the gasifier system which could be interfered from contemplating
417 in Figs 3a and 3b. Also by an increase in current density, the value of heating capacity increases
418 by up to 83% and 45% for the G-SOFC system and D-SOFC system respectively.

419 Fig. 4 shows the effect of current density on the unit exergy cost of power output (c_w) and hot
420 steam (c_h) for both the D-SOFC and G-SOFC systems. It is revealed that besides the efficiency
421 of D-SOFC is higher it has come at the price of lower unit product cost. Also it is unfolded that
422 for both cases the unit product cost is minimized at some specific point. For the G-SOFC system,
423 the minimum value of unit exergy cost of heating (24.67$/GJ) occurs at current density of 0.203
424 A/cm^2 while for the case of D-SOFC system the values are 14.17 $/GJ and 0.602 A/cm^2,
425 respectively. It can be seen that even in the minimum values, the D-SOFC system is cost-
426 efficient by 41.6% and 70.2% for heating unit exergy cost and power unit exergy cost,
427 respectively.

Another key parameter having effect on the system performance is the stack temperature difference. Fig. 5 shows the effect of stack temperature difference on second law efficiency of CHP and power generation systems for both the D-SOFC and G-SOFC systems. Second law efficiency for the D-SOFC system is always higher than that for the G-SOFC system but important aspect of this figure is that variation of second law efficiency for power generation mode and CHP mode of G-SOFC tends to decrease after a specific value of temperature. This is actually due to the different composition of inlet gas sent to the anode and consequently different partial pressure of H_2 and H_2O at the anode exit. As the stack temperature difference increases 110 ^oC, exergetic efficiency for D-SOFC system (in the CHP mode) rises by 52.9% while with an increase of 90^oC the efficiency of the G-SOFC system increases by 75.3%. In addition, as the temperature difference increases by 80 ^oC the second law efficiency of power generation system for the G-SOFC system rises by 25%, the change is an almost the same for the case of D-SOFC with a value of 25.4%.

Fig. 6a shows the effect of stack temperature difference on the net power output and heating capacity for the D-SOFC and G-SOFC systems. Comparing the G-SOFC and D-SOFC systems, net power output of G-SOFC system increases by 27.60% with an increase in stack temperature difference and for the D-SOFC system the increase is 25.5%. The trend of heat duty is different as with an increase in temperature of stack results in an increase of exhaust potential of SOFC system which would be utilized in HRSG system. Although the trend seems to be similar for two cases, for the D-SOFC system the percentage of increase is much higher compared to the G-SOFC system.

Fig. 6b shows the effect of stack temperature difference on unit exergy costs of heating capacity and power output for both the D-SOFC and G-SOFC systems. It is revealed that for the

D-SOFC system unit heating product cost is minimized at stack temperature difference of 183 K which corresponds to unit cost of 9.18 $/GJ while the stack temperature difference and unit cost values are 135.6 K and 16.1 $/GJ for the G-SOFC system. Also, at the minimum point the D-SOFC system has 75.3% less unit product cost in heating and 91.31% in power unit product cost compared to the G-SOFC system.

Finally to give an insight of overall product cost variation with terminal temperature differences of SOFC stack Fig. 6c is presented. It shows that the with a change of about 100 ^{o}C in stack temperature difference, the minimum unit product cost of G-SOFC system is more than the maximum unit product cost of D-SOFC system.

Fig. 7a and Fig. 7b illustrate the G-SOFC and D-SOFC systems' calculated parameters at nominal operating condition and stack temperature difference equal to 100 ^{o}C. According to Fig. 7a the second law efficiency for the D-SOFC system is higher with a value of 97.8% in power generation system and 57.7% in CHP system. The difference becomes less in CHP system due to higher heating capacity in G-SOFC system, moreover considering the results illustrated in Fig. 7b it is found that the unit product cost for G-SOFC system for power generation system and CHP system is 42.6% and 24.5% more than those for the D-SOFC system respectively. Fig. 7b shows the value of net output power and heating capacity as well as the unit product cost for power and heating for the two proposed systems at the same working conditions. Fig.7b shows that the G-SOFC system has 111 kW less power output and 45.9kW more heating load than the D-SOFC system.

One method to illustrate exergy accounting graphically is the Grassman diagram [48]. The width of the arrows entering or leaving the control volume is a quantitative measure of designated parameter. Also for the sake of brevity, values of exergy destruction along with

entering and leaving exergy to the whole system are presented in Table 6. According to the Figs. 8a and 8b and Table 6, one may conclude that the air heat exchanger and the gasifier are the main sources of irreversibility due to the existence of three sources of irreversibility (temperature difference, chemical reaction along with system friction) within these components in the D-SOFC and G-SOFC systems respectively.

Table 7 and Table 8 show the exergoeconomic analysis results for the G-SOFC and D-SOFC systems. Last column of these tables is exergoeconomic factor which a low value of this factor calculated for a major component suggests that cost saving in the entire system *might* be achieved by improving the component efficiency (reducing exergy destruction) even if the capital investment for the component will increase. However, the exergoeconomic factor is not sufficient to explain if a component has to be modified or not. As an example: even if a component has a too low value of exergoeconomic factor (suggesting therefore its substitution with a component of higher performance and higher cost) if the same component elaborates a quantity of fuel which is negligible (and so it has a low value of the so called exergetic factor) it is not worth at all to substitute this component with a better one, as its "exergy role" on the system is simply negligible. The most important components to discuss are the components elaborating a large amount of inlet fuel (so, which have a high value of exergetic factor): only in their case it is interesting to analyze the values of their exergoeconomic factor. Referring to first column of Tables 7 and 8, it can be noted that for the gasifier based system, among the components having higher inlet exergy (SOFC stack, gasfier, after burner and AHX respectively) the SOFC stack and AHX have the highest (88.75%) and lowest (16.02%) exergoeconomic factors, respectively. Therefore, for the case of G-SOFC system, on the one hand, engineers should focus on reducing the investment and operation costs of SOFC stack and on the other

hand, they are to reduce the costs associated with exergy destruction for the AHX. The same point can be stated for the case of D-SOFC. Therefore, for the D-SOFC and G-SOFC systems, not only designers should emphasize on decreasing the investment cost of SOFC stack but also reducing the cost associated with exergy destruction within the air heat exchangers should be in priority.

Finally at the end, a summary of plant type, fuel type and technology of using biomass to produce gas to feed SOFC power plant in some published works as well as those proposed and obtained in the present work are listed in Table 9. Comparison shows that most of the published works focused on just one technology (gasification to produce syngas or digestion to produce biogas) to utilize the biomass. Also there are few works that comprehensively analyzed the system from the both of thermodynamic and techno economic point of view. However, in the present work, the investigation has been made to fulfill this gap and the thermodynamic and economic analyses are performed to compare two well-known technologies of using biomass in the SOFC system.

7. Conclusion

A comprehensive thermodynamic and thermoeconomic modeling are performed for two proposed cogeneration systems based on SOFC system fed by municipal solid waste. The inlet fuel for the SOFC is a type of syngas produced by gasification process of municipal solid waste or a biogas produced by digestion process. For the comparison purposes, the systems analyzed in two modes; one-generation system (produce power) and a CHP mode (producing power and heating simultaneously). Parametric studies revealed that stack temperature difference along with current density has crucial effect on systems' performance. Additional conclusions are as

519 follows:

520 • D-SOFC system has higher efficiency from the viewpoints of energy and exergy when
521 the systems run to produce power.
522 • D-SOFC system has higher second law efficiency in CHP mode; however the first law
523 efficiency for the G-SOFC is higher in this mode.
524 • D-SOFC system has more power output but less heating capacity compared to those of
525 the G-SOFC system.
526 • For the case of G-SOFC system the gasifier is the main source of irreversibility due to
527 temperature difference and chemical reaction. Meanwhile, air heat exchanger is the
528 second source of irreversibility because of large temperature difference on the both sides
529 of heat exchanger. For the D-SOFC system, air heat exchanger has the most distribution
530 in exergy destruction within the system, the stack and digester are the second and third
531 respectively.

532

533

534

535 **Appendix A**

536 Here, the electrochemical model (for calculating the cell voltage) programing in EES is given
537 in details. The cell voltage can be defined as;

$$V_c = V_N - V_{loss} \quad \text{(A1)}$$

538 where, V_N is the Nernst voltage and V_{loss} is the voltage loss which is the sum of three

$$V_{loss} = V_{ohm} + V_{act} + V_{conc} \quad \text{(A2)}$$

539 separate voltage losses (ohmic, activation, and concentration losses):

$$V_N = -\frac{\Delta \bar{g}^o}{2F} + \frac{\bar{R}T_{FC,e}}{2F} \ln\left(\frac{a_{H_2}^{Anode,exit} \sqrt{a_{O_2}^{Cathode,exit}}}{a_{H_2O}^{Anode,exit}} \right) \quad \text{(A3)}$$

540 The Nernst voltage which is accounted as the ideal voltage can be expressed as;

541 In equation (A3), the Gibbs energy difference is related to the overall electrochemical
542 reaction. To determine the actual cell voltage, the voltage losses should be calculated. To
543 calculate the Ohmic loss the following formula is used [52];

$$V_{ohm} = (R_{Int} + \rho_{an} L_{an} + \rho_{cat} L_{cat} + \rho_{ely} L_{ely})\, j \quad \text{(A4)}$$

544 where, ρ, L and R_{Int} denote electrical resistivity of a cell component, thickness of a cell
545 component and interconnection resistivity, respectively (See Table A.1).

546 The activation polarization is the sum of those defined for both the anode and cathode as
547 follows;

$$V_{act} = V_{act,a} + V_{act,c} \quad \text{A5}$$

$$V_{act,c} = \frac{\bar{R}T_{FC,e}}{F}(\sinh^{-1}(\frac{j}{2j_{oa}})) \quad \text{A6}$$

$$V_{act,c} = \frac{\bar{R}T_{FC,e}}{F}(\sinh^{-1}(\frac{j}{2j_{oc}})) \quad \text{A7}$$

548 Where j_o is the exchange current density. Eqs. (A8) and (A9) are used to evaluate the values
549 of the exchange current density for the anode and the cathode, (see variables in Table A.2),

$$j_{0,a} = \gamma_{an}\ (\frac{RT}{2F})\, e^{\left(-\frac{E_{a,an}}{\bar{R}T}\right)} \quad \text{A8}$$

$$j_{0,c} = \gamma_{cat}\ (\frac{RT}{2F})\, e^{\left(-\frac{E_{a,cat}}{\bar{R}T}\right)} \quad \text{A9}$$

550 respectively [52].

551 Concentration loss is sum of the losses related to gas concentration occurring in the anode

$$V_{conc} = V_{conc,a} + V_{conc,c} \quad \text{A10}$$

552 and cathode.

$$V_{conc,an} = \frac{RT}{2F}\ln(\frac{P_{H_2}\ P_{H_2O,TPB}}{P_{H_2O}\ P_{H_2,TPB}}) \quad \text{A11}$$

553 Where

$$V_{conc,cat} = \frac{RT}{4F}\log(\frac{P_{O_2}}{P_{O_2,TPB}}) \quad \text{A12}$$

554 And

555 where the subscript *TPB* denotes the three-phase boundary. To calculate the pressure at the

$$P_{H_2O,TPB} = P_{H_2O,an} + j\,\frac{R\,T\;L_{an}}{2\,F\,D^{eff}_{an,H_2}} \quad \text{A13}$$

556 reaction sites, the following equations have been used [52,53]:

$$P_{H_2,TPB} = P_{H_2,an} - j\,\frac{R\,T\;L_{an}}{2\,F\,D^{eff}_{an,H_2O}} \quad \text{A14}$$

$$P_{O_2,TPB} = P_{cat} - (P_{cat} - P_{O_2,cat})\exp(j\,\frac{RT\;L_{cat}}{4F\,D^{eff}_{O_2}\,p_{cat}}) \quad \text{A15}$$

557

558 where, $D^{eff}_{H_2}$, $D^{eff}_{H_2O}$ and $D^{eff}_{O_2}$ are the effective gaseous diffusivity through the anode (for H_2),

559 anode (for H_2O) and the cathode (for O_2), respectively. The effective gaseous diffusivity can be

$$\frac{1}{D^{eff}_{an,H_2}} = \frac{\varepsilon_{an}}{\tau_{an}}(\frac{1}{D_{H_2,K}} + \frac{1}{D_{H_2,H_2O}}) \quad \text{A16}$$

$$\frac{1}{D^{eff}_{an,H_2O}} = \frac{\varepsilon_{an}}{\tau_{an}}(\frac{1}{D_{H_2O,K}} + \frac{1}{D_{H_2O,H_2}}) \quad \text{A17}$$

$$\frac{1}{D^{eff}_{\mathrm{cat},O_2}} = \frac{\varepsilon_{cat}}{\tau_{cat}}(\frac{1}{D_{O_2,K}} + \frac{1}{D_{O_2,N_2}}) \quad \text{A18}$$

560 calculated as [52,53];

561 Where the porosity (ε) and tortuosity (τ) of electrode materials are estimated to be 0.48 and

562 5.4, respectively. To calculate the effective gaseous diffusivity, combined ordinary and Knudsen

563 diffusion should be defined and calculated using the following equations as[52];

$$D_{H_2,K} = 97 r_{pore,an} \sqrt{\frac{T}{M_{H2}}} \quad \text{A19}$$

$$D_{H_2O,K} = 97 r_{pore,an} \sqrt{\frac{T}{M_{H_2O}}} \quad \text{A20}$$

$$D_{O_2,K} = 97 r_{pore,cat} \sqrt{\frac{T}{M_{O_2}}} \quad \text{A21}$$

$$D_{H_2,H_2O} = \frac{1.43\times10^{-7} T^{1.75}}{\sqrt{M_{H_2,H_2O}} (V_{H_2}^{1/3} + V_{H_2O}^{1/3})^2 P} \quad \text{A22}$$

$$D_{O_2,N_2} = \frac{1.43\times10^{-7} T^{1.75}}{\sqrt{M_{O_2,N_2}} (V_{O_2}^{1/3} + V_{N_2}^{1/3})^2 P} \quad \text{A23}$$

Where M is molecular weight of species, V represents diffusion volume of species. Meanwhile, pore radius value (r_{pore}) is estimated to be $0.5\,\mu m$.

References

[1] Basu P. Combustion and gasification in fluidized beds. Broken Sound Parkway NW, Suit 300: CRC press (Taylor and Francis); 2006.

[2] Basu P. Biomass gasification, pyrolysis and torrefaction: practical design and theory. 2nd ed. 32 Jamestown Road, London NW1 7BY, UK: Academic press (Elsevier); 2013.

[3] Mckendry P. Energy production from biomass (part 3): gasification technologies. Bioresour Technol 2002;83:55–63.

[4] Mckendry P. Energy production from biomass (part 1): overview of biomass. Bioresour Technol 2002;83:37–46.

[5] Mckendry P. Energy production from biomass (part 2): conversion technologies. Bioresour Technol 2002;83:47–54.

[6] Soltani S, Yari M, Mahmoudi SMS, Morosuk T, Rosen MA. Advanced exergy analysis applied to an externally-fired combined-cycle power plant integrated with a biomass gasification unit. Energy 2013;59:775–80.

[7] Saidur R, Abdelaziz EA, Demirbas A, Hossain MS, Mekhilef S. A review on biomass as a fuel for boilers. Renew Sustain Energy Rev 2011;15:2262–89.

[8] Yoshioka T, Hirata S, Matsumura Y, Sakanishi K. Woody biomass resources and conversion in Japan: The current situation and projections to 2010 and 2050. Biomass and Bioenergy 2005;29:336–46.

[9] Sebastián F, Royo J, Gómez M. Cofiring versus biomass-fired power plants: GHG (Greenhouse Gases) emissions savings comparison by means of LCA (Life Cycle Assessment) methodology. Energy 2011;36:2029–37.

[10] Karamarkovic R, Karamarkovic V. Energy and exergy analysis of biomass gasification at different temperatures. Energy 2010;35:537–49.

[11] Soltani S, Mahmoudi SMS, Yari M, Rosen MA. Thermodynamic analyses of a biomass integrated fired combined cycle. Appl Therm Eng 2013;59:60–8.

[12] Warnecke R. Gasification of biomass: comparison of fixed bed and fluidized bed gasifier.

Biomass and Bioenergy 2000;18:489–97.

[13] Knoef HAM. Inventory of biomass gasifier manufacturers and installations. Final Report to European Commission. Contract DIS/1734/98-NL, Biomass Technol Gr BV, Univ Twente, Enschede 2000.

[14] Omosun AO, Bauen A, Brandon NP, Adjiman CS, Hart D. Modelling system efficiencies and costs of two biomass-fuelled SOFC systems. J Power Sources 2004;131:96–106.

[15] Singh D, Hernández-Pacheco E, Hutton PN, Patel N, Mann MD. Carbon deposition in an SOFC fueled by tar-laden biomass gas: A thermodynamic analysis. J Power Sources 2005;142:194–9.

[16] Athanasiou C, Coutelieris F, Vakouftsi E, Skoulou V, Antonakou E, Marnellos G, et al. From biomass to electricity through integrated gasification/SOFC system-optimization and energy balance. Int J Hydrogen Energy 2007;32:337–42.

[17] Colpan CO, Dincer I, Hamdullahpur F. Thermodynamic modeling of direct internal reforming solid oxide fuel cells operating with syngas. Int J Hydrogen Energy 2007;32:787–95.

[18] Jang H, Ocon JD, Lee S, Lee JK, Lee J. Direct power generation from waste coffee grounds in a biomass fuel cell. J Power Sources 2015;296:433–9.

[19] Pieratti E, Baratieri M, Ceschini S, Tognana L, Baggio P. Syngas suitability for solid oxide fuel cells applications produced via biomass steam gasification process: Experimental and modeling analysis. J Power Sources 2011;196:10038–49.

[20] Di Carlo A, Bocci E, Naso V. Process simulation of a SOFC and double bubbling fluidized bed gasifier power plant. Int J Hydrogen Energy 2013;38:532–42.

[21] De Lorenzo G, Fragiacomo P. Energy analysis of an SOFC system fed by syngas. Energy Convers Manag 2015;93:175–86.

[22] Jia J, Abudula A, Wei L, Sun B, Shi Y. Thermodynamic modeling of an integrated biomass gasification and solid oxide fuel cell system. Renew Energy 2015;81:400–10.

[23] Jia J, Abudula A, Wei L, Sun B, Shi Y. Effect of operating parameters on performance of an integrated biomass gasifier, solid oxide fuel cells and micro gas turbine system.

Biomass and Bioenergy 2015;75:35–45.

[24] Kartha S, Kreutz TG, Williams RH. Small-scale biomass fuel cell/gas turbine power systems for rural areas. Energy Sustain Dev 2000;4:85–9.

[25] Ghirardo F, Santin M, Traverso A, Massardo A. Heat recovery options for onboard fuel cell systems. Int J Hydrogen Energy 2011;36:8134–42.

[26] Piroonlerkgul P, Assabumrungrat S, Laosiripojana N, Adesina AA. Selection of appropriate fuel processor for biogas-fuelled SOFC system. Chem Eng J 2008;140:341–51.

[27] Farhad S, Hamdullahpur F, Yoo Y. Performance evaluation of different configurations of biogas-fuelled SOFC micro-CHP systems for residential applications. Int J Hydrogen Energy 2010;35:3758–68.

[28] Tjaden B, Gandiglio M, Lanzini A, Santarelli M, Järvinen M. Small-Scale Biogas-SOFC Plant: Technical Analysis and Assessment of Different Fuel Reforming Options. Energy & Fuels 2014;28:4216–32.

[29] Santarelli M, Barra S, Sagnelli F, Zitella P. Biomass-to-electricity: Analysis and optimization of the complete pathway steam explosion - enzymatic hydrolysis - anaerobic digestion with ICE vs SOFC as biogas users. Bioresour Technol 2012;123:430–8.

[30] Papurello D, Lanzini A, Tognana L, Silvestri S, Santarelli M. Waste to energy: Exploitation of biogas from organic waste in a 500 Wel solid oxide fuel cell (SOFC) stack. Energy 2015;85:145–58.

[31] Trendewicz a. a., Braun RJ. Techno-economic analysis of solid oxide fuel cell-based combined heat and power systems for biogas utilization at wastewater treatment facilities. J Power Sources 2013;233:380–93.

[32] Gandiglio M, Lanzini A, Santarelli M, Leone P. Design and Balance-of-Plant of a Demonstration Plant With a Solid Oxide Fuel Cell Fed by Biogas From Waste-Water and Exhaust Carbon Recycling for Algae Growth. J Fuel Cell Sci Technol 2014;11:031003.

[33] Siefert NS, Litster S. Exergy & economic analysis of biogas fueled solid oxide fuel cell systems. J Power Sources 2014;272:386–97.

[34] Mehr AS, Mahmoudi SMS, Yari M, Chitsaz A. Thermodynamic and exergoeconomic analysis of biogas fed solid oxide fuel cell power plants emphasizing on anode and cathode recycling: A comparative study. Energy Convers Manag 2015;105:596–606.

[35] Ranjbar F, Chitsaz A, Mahmoudi SMS, Khalilarya S, Rosen MA. Energy and exergy assessments of a novel trigeneration system based on a solid oxide fuel cell. Energy Convers Manag 2014;87:318–27.

[36] Soltani S, Mahmoudi SMS, Yari M, Rosen MA. Thermodynamic analyses of an externally fired gas turbine combined cycle integrated with a biomass gasification plant. Energy Convers Manag 2013;70:107–15.

[37] Al-Sulaiman FA, Dincer I, Hamdullahpur F. Energy analysis of a trigeneration plant based on solid oxide fuel cell and organic Rankine cycle. Int J Hydrogen Energy 2010;35:5104–13.

[38] Landau L, Moran MJ, Shapiro HN, Boettner DD, Bailey M. Fundamentals of engineering thermodynamics. John Wiley & Sons; 2010.

[39] Gholamian E, Mahmoudi SMS, Zare V. Proposal, exergy analysis and optimization of a new biomass-based cogeneration system. Appl Therm Eng 2016;93:223–35.

[40] Zainal ZA, Ali R, Lean CH, Seetharamu KN. Prediction of performance of a downdraft gasifier using equilibrium modeling for different biomass materials. Energy Convers Manag 2001;42:1499–515.

[41] Jayah TH, Aye L, Fuller RJ, Stewart DF. Computer simulation of a downdraft wood gasifier for tea drying. Biomass and Bioenergy 2003;25:459–69.

[42] Jarungthammachote S, Dutta A. Thermodynamic equilibrium model and second law analysis of a downdraft waste gasifier. Energy 2007;32:1660–9.

[43] Tao G, Armstrong T, Virkar A. Intermediate temperature solid oxide fuel cell (IT-SOFC) research and development activities at MSRI. Ninet. Annu. ACERC&ICES Conf. Utah, 2005.

[44] Buswell AM, Hatfield WD. Anaerobic fermentations. Bull 1936;32.

[45] Wellinger A, Murphy JD, Baxter D. The biogas handbook: science, production and

applications. Elsevier; 2013.

[46] Ryu C, Yang Y Bin, Khor A, Yates NE, Sharifi VN, Swithenbank J. Effect of fuel properties on biomass combustion: Part I. Experiments-fuel type, equivalence ratio and particle size. Fuel 2006;85:1039–46.

[47] Chan SH, Ho HK, Tian Y. Modelling of simple hybrid solid oxide fuel cell and gas turbine power plant. J Power Sources 2002;109:111–20.

[48] Bejan A, Moran MJ. Thermal design and optimization. John Wiley & Sons; 1996.

[49] Ahmadi P, Dincer I, Rosen MA. Development and assessment of an integrated biomass-based multi-generation energy system. Energy 2013;56:155–66.

[50] Tsatsaronis G, Lin L, Pisa J. Exergy costing in exergoeconomics. J Energy Resour Technol 1993;115:9–16.

[51] Mehr AS, Zare V, Mahmoudi SMS. Standard GAX versus hybrid GAX absorption refrigeration cycle: From the view point of thermoeconomics. Energy Convers Manag 2013;76:68–82.

[52] Wongchanapai S, Iwai H, Saito M, Yoshida H. Selection of suitable operating conditions for planar anode-supported direct-internal-reforming solid-oxide fuel cell. J Power Sources 2012;204:14–24.

[53] Lanzini A, Santarelli M, Orsello G. Residential solid oxide fuel cell generator fuelled by ethanol: Cell, stack and systemmodelling with a preliminary experiment. Fuel Cells 2010;10:654–75.

[54] Madi H, Lanzini A, Diethelm S, Papurello D, Van herle J, Lualdi M, et al. Solid oxide fuel cell anode degradation by the effect of siloxanes. J Power Sources 2015;279:460–71. doi:10.1016/j.jpowsour.2015.01.053.

[55] Al-Sulaiman FA, Dincer I, Hamdullahpur F. Energy and exergy analyses of a biomass trigeneration system using an organic Rankine cycle. Energy 2012;45:975–85.

[56] Farhad S, Yoo Y, Hamdullahpur F. Effects of fuel processing methods on industrial scale biogas-fuelled solid oxide fuel cell system for operating in wastewater treatment plants 2010;195:1446–53.

[57] Bang-Møller C, Rokni M, Elmegaard B. Exergy analysis and optimization of a biomass gasification, solid oxide fuel cell and micro gas turbine hybrid system. Energy 2011;36:4740–52.

[58] El-Emam RS, Dincer I, Naterer GF. Energy and exergy analyses of an integrated SOFC and coal gasification system. Int J Hydrogen Energy 2012;37:1689–97.

[59] Wongchanapai S, Iwai H, Saito M, Yoshida H. Performance evaluation of an integrated small-scale SOFC-biomass gasification power generation system. J Power Sources 2012;216:314–22.

[60] Campitelli G, Cordiner S, Gautam M, Mariani A, Mulone V. Biomass fueling of a SOFC by integrated gasifier: Study of the effect of operating conditions on system performance. Int J Hydrogen Energy 2013;38:320–7.

[61] Arteaga-Pérez LE, Casas-Ledón Y, Pérez-Bermúdez R, Peralta LM, Dewulf J, Prins W. Energy and exergy analysis of a sugar cane bagasse gasifier integrated to a solid oxide fuel cell based on a quasi-equilibrium approach. Chem Eng J 2013;228:1121–32.

[62] Morandin M, Maréchal F, Giacomini S. Synthesis and thermo-economic design optimization of wood-gasifier-SOFC systems for small scale applications. Biomass and Bioenergy 2013;49:299–314.

[63] Ozcan H, Dincer I. Performance evaluation of an SOFC based trigeneration system using various gaseous fuels from biomass gasification. Int J Hydrogen Energy 2014:1–10.

[64] Caliandro P, Tock L, Ensinas A V., Marechal F. Thermo-economic optimization of a Solid Oxide Fuel Cell - Gas turbine system fuelled with gasified lignocellulosic biomass. Energy Convers Manag 2014;85:764–73.

[65] Curletti F, Gandiglio M, Lanzini A, Santarelli M. Large size biogas-fed Solid Oxide Fuel Cell power plants with carbon dioxide management : Technical and economic optimization 2015;294.

[66] Lv X, Liu X, Gu C, Weng Y. Determination of safe operation zone for an intermediate-temperature solid oxide fuel cell and gas turbine hybrid system. Energy 2016;99:91–102.

Figures' caption

Figure 1 schematic diagram of CHP system based on a) digester coupled SOFC, b) gasifier coupled SOFC

Figure 2 Effect of current density on first and second law efficiencies of power generating system

Figure 3 Effect of current density on a) first and second law efficiencies of CHP system b) net power output and heating value of CHP system

Figure 4 effect of current density unit product cost of heat and power

Figure 5 Effect of stack temperature difference on second law efficiency of power generating and CHP system

Figure 6 effect of stack temperature difference on a) net power output and heating capacity b) unit product cost of heating and power c) total product cost of digester coupled SOFC and gasifier coupled SOFC

Figure 7 Comparison of a) first and second law efficiencies of systems as well as the total product cost b) net output power and heating load of systems as well as the their product costs

Figure 8 Grassman diagram of the a) digester coupled CHP system based on SOFC (D-SOFC) b) gasifier coupled CHP system based on SOFC (G-SOFC)

Tables' Caption

Table 1. Input data for the SOFC systems [34,37,45,55]
Table 2 Ultimate analysis of MSW [39]
Table 2. The comparison of the component percentages in the producer gas obtained from the gasification in the present work and those reported in the literature, for wood with a moisture content of 16% and for a gasification temperature of 1100K.
Table 3. Comparison of results obtained from the present work with the experimental values reported by Tao et al. [43]
Table 4 Input data* and cost and auxiliary equations for each component [11,33]
Table 6. Exergy and exergy destruction rates for two proposed SOFC systems
Table 7 Exergoeconomic analysis results for the gasifier coupled SOFC
Table 8 Exergoeconomic analysis results for the Digester coupled SOFC
Table A.1. Material Resistivity used for ohmic voltage loss estimation [52]
Table A.2. Parameters correspond to anode and cathode sides material [52]

859

860 **Figures**

a)

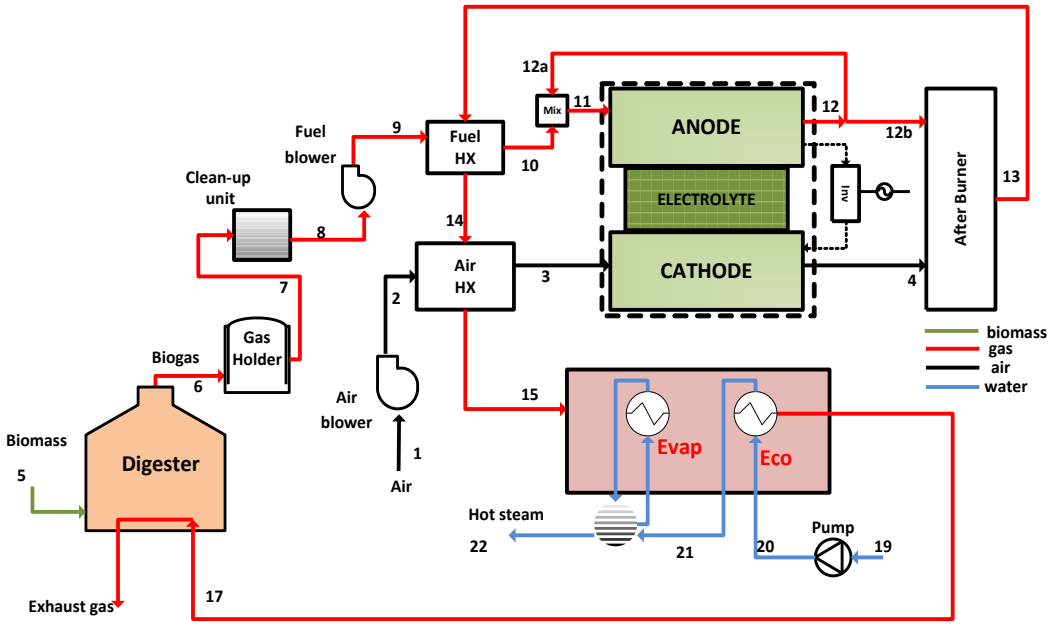

b)

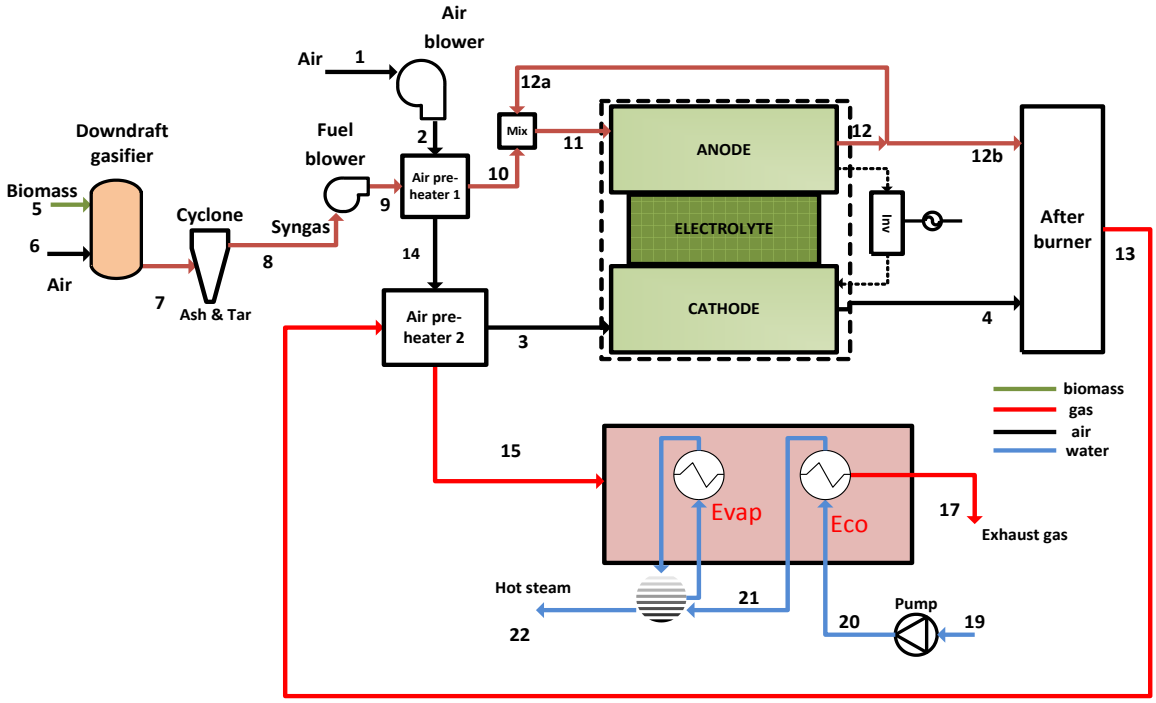

Figure 1 schematic diagram of CHP system based on a) digester coupled SOFC, b) gasifier coupled SOFC

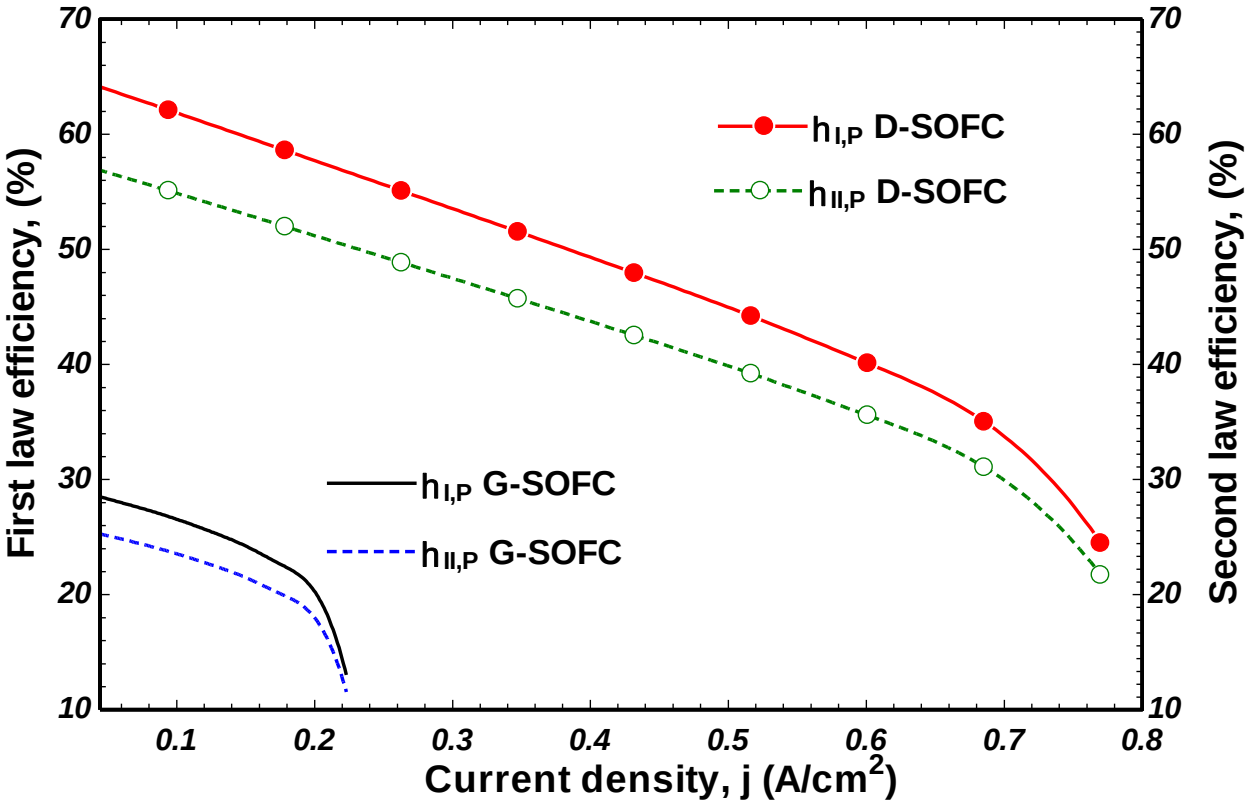

Figure 2 Effect of current density on first and second law efficiencies of power generating system

871

a)

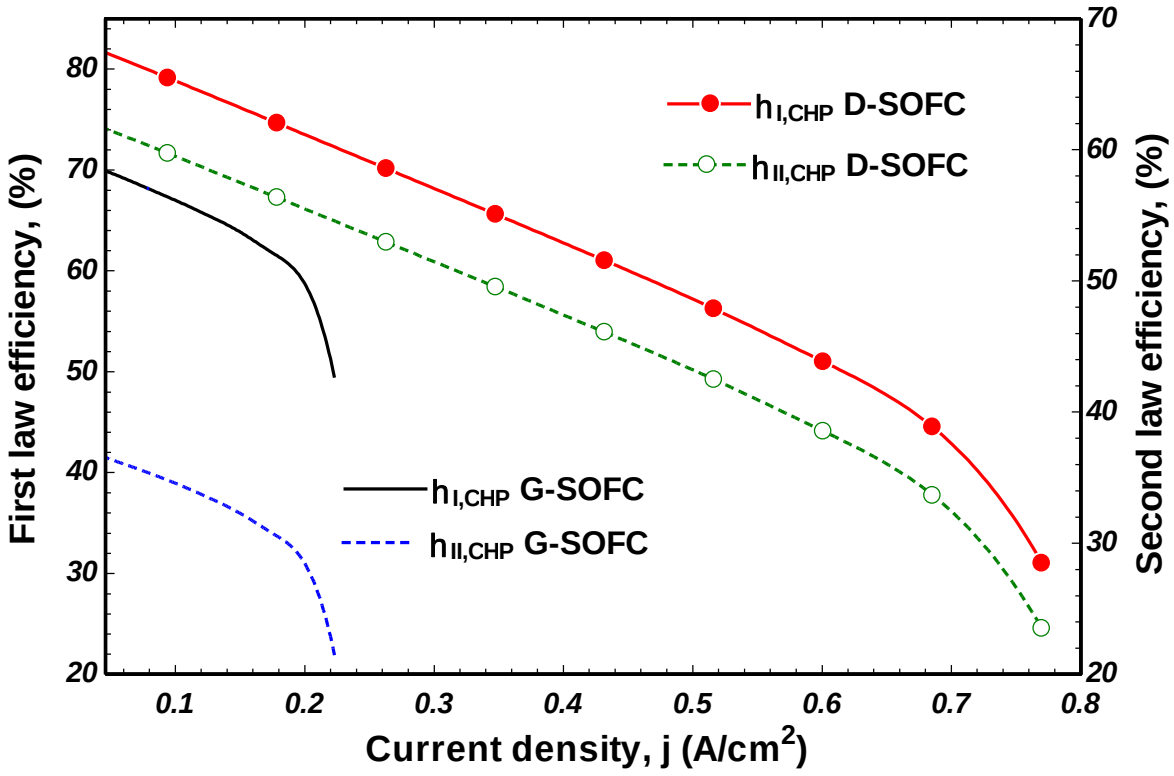
First law efficiency, (%)
Second law efficiency, (%)
Current density, j (A/cm2)
hI,CHP D-SOFC
hII,CHP D-SOFC
hI,CHP G-SOFC
hII,CHP G-SOFC
80
70
60
50
40
30
20
70
60
50
40
30
20
0.1
0.2
0.3
0.4
0.5
0.6
0.7
0.8

b)

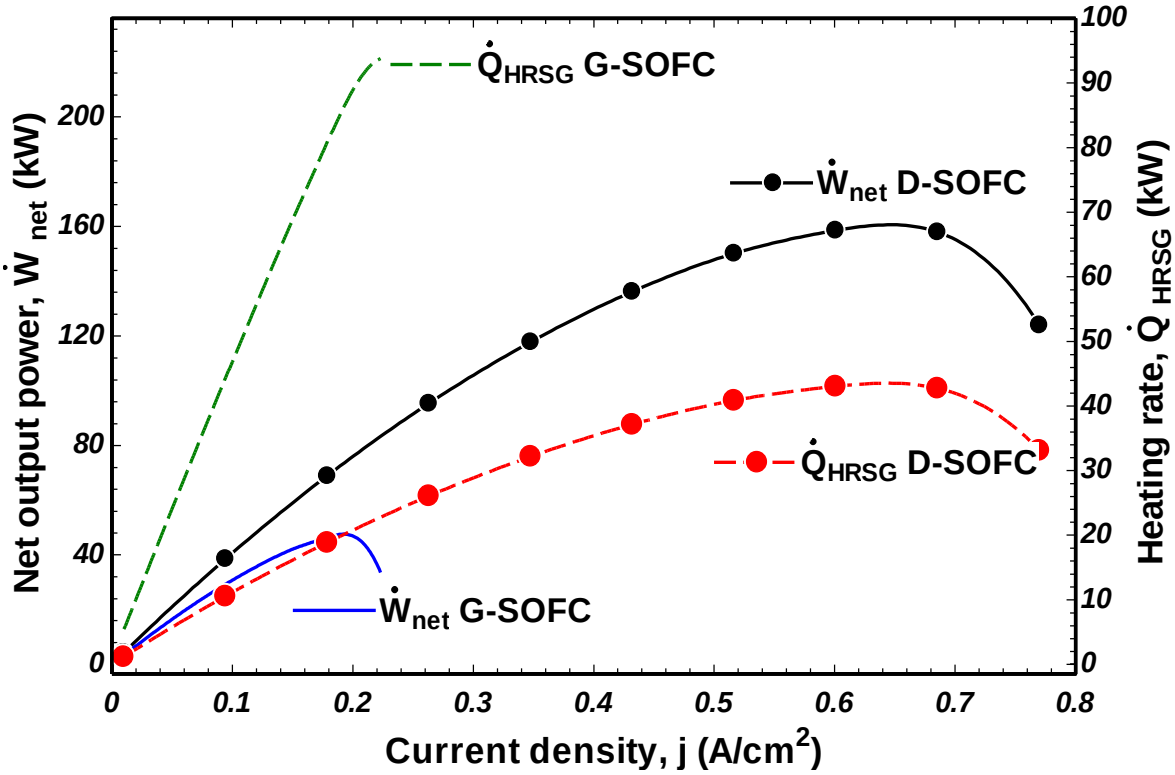

Figure 3 Effect of current density on a) first and second law efficiencies of CHP system b) net power output and heating value of CHP system

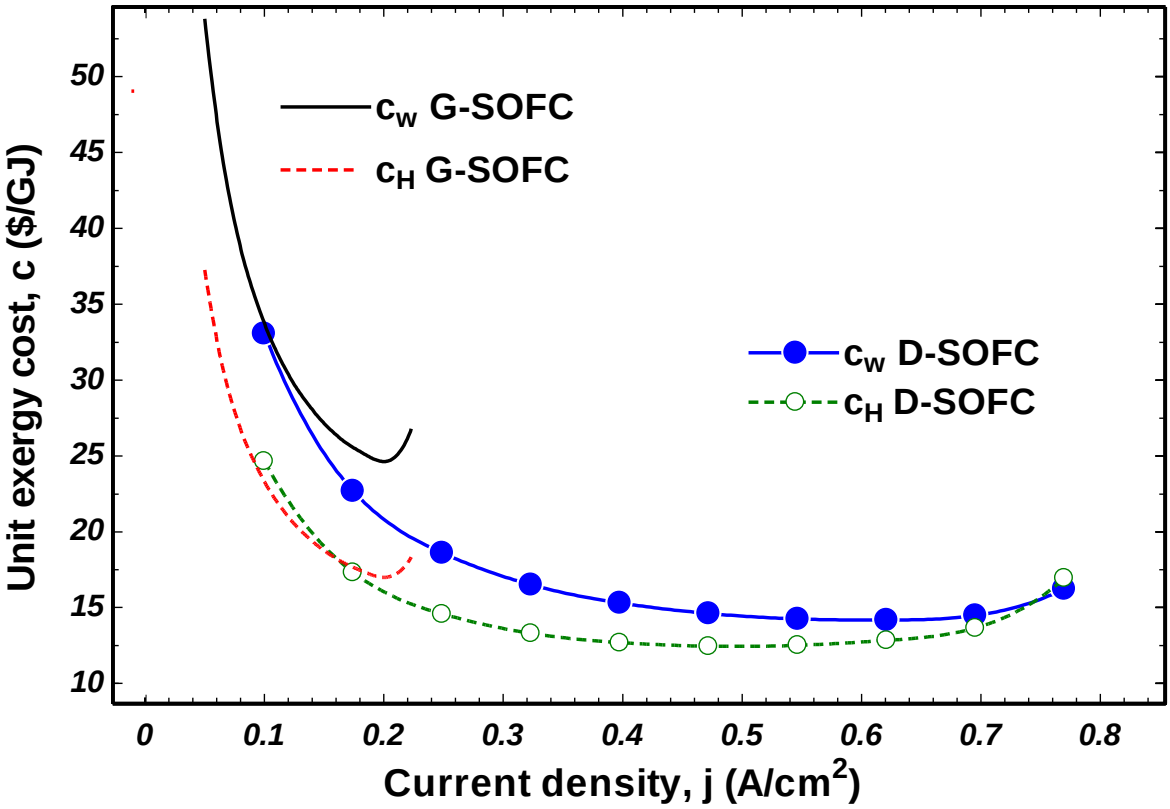

885

886 Figure 4 effect of current density unit product cost of heat and power

887

888

889

890

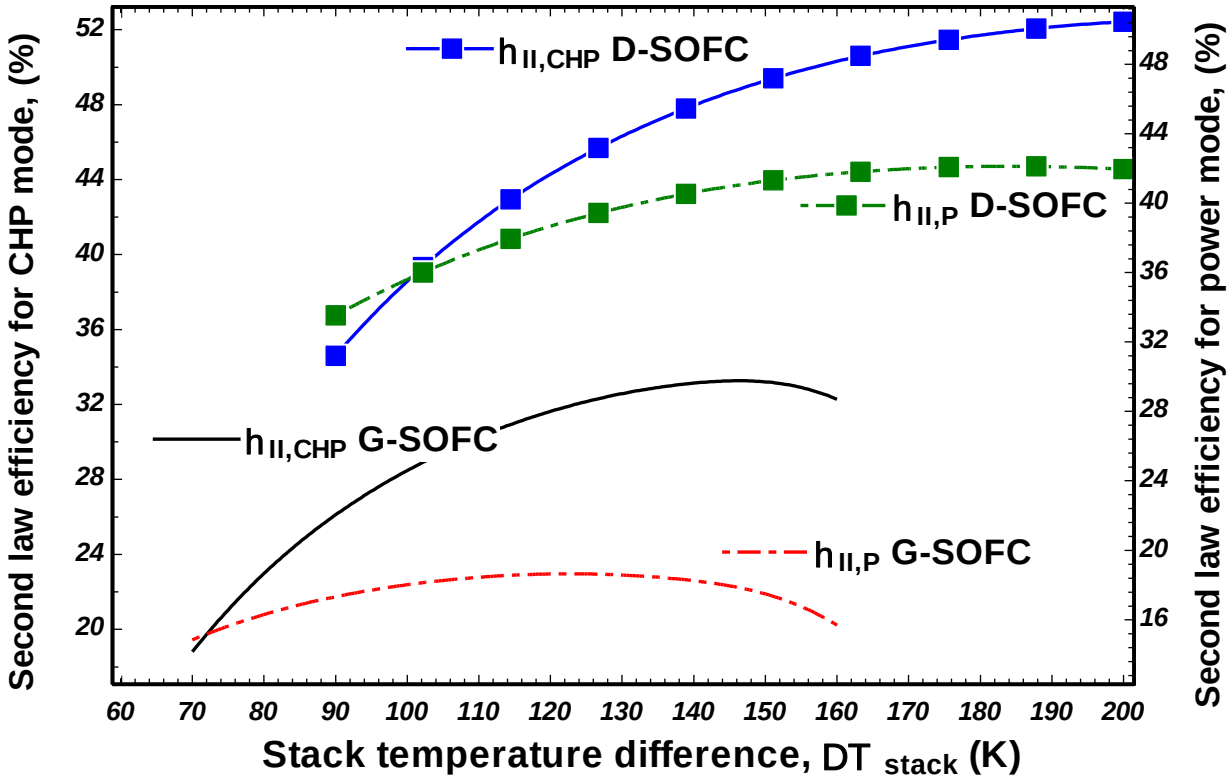

891

892 Figure 5 Effect of stack temperature difference on second law efficiency of power generating and CHP
893 system

894

895

896

897

a)

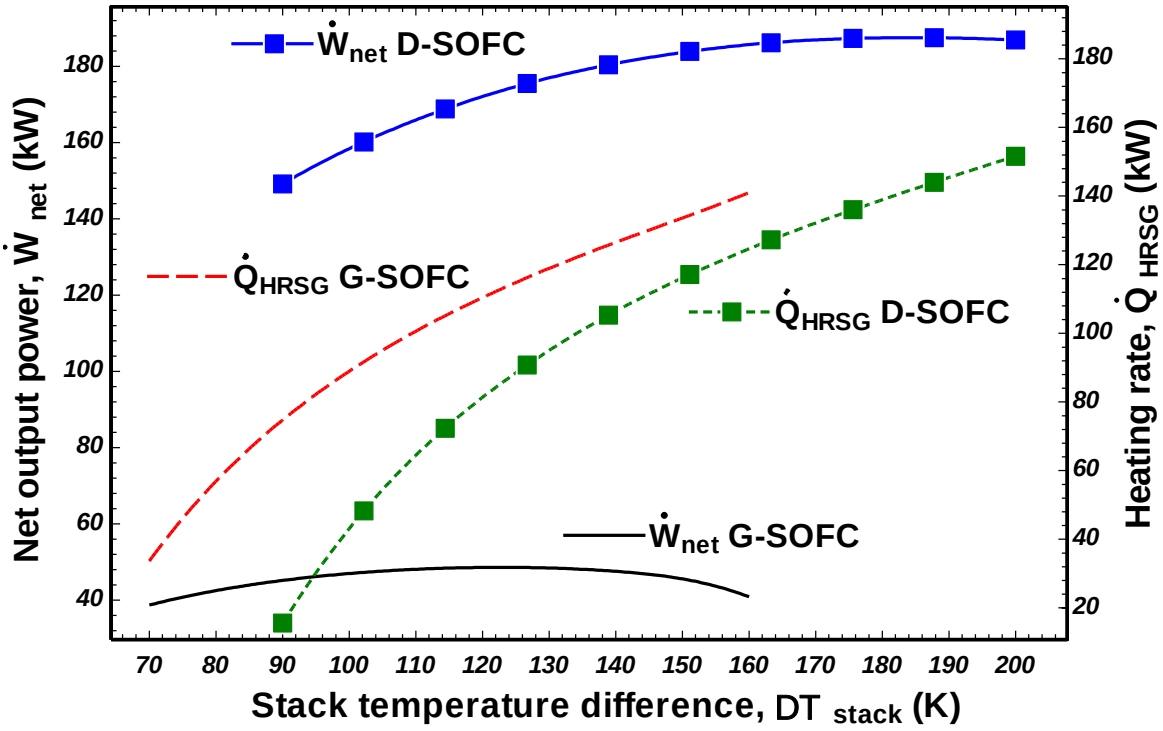
Ẇnet D-SOFC
Q̇HRSG G-SOFC
Q̇HRSG D-SOFC
Ẇnet G-SOFC
Net output power, Ẇ net (kW)
Heating rate, Q̇ HRSG (kW)
Stack temperature difference, DT stack (K)
40
60
80
100
120
140
160
180
20
40
60
80
100
120
140
160
180
70
80
90
100
110
120
130
140
150
160
170
180
190
200

b)

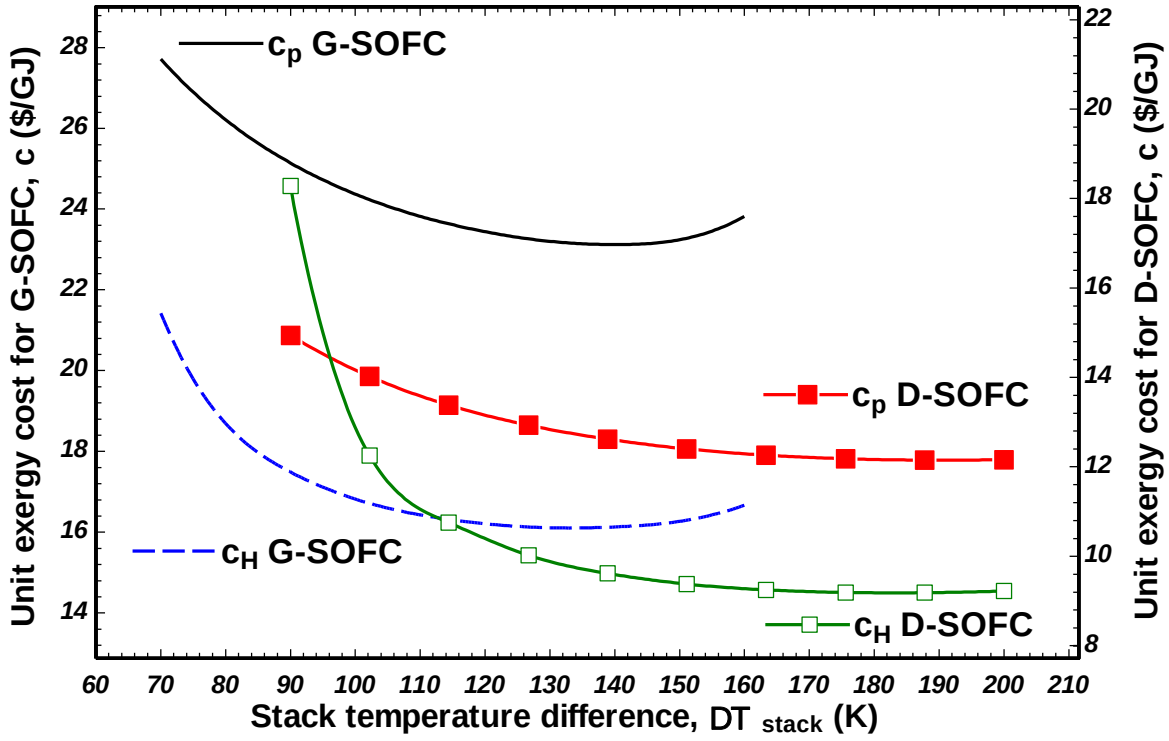

c)

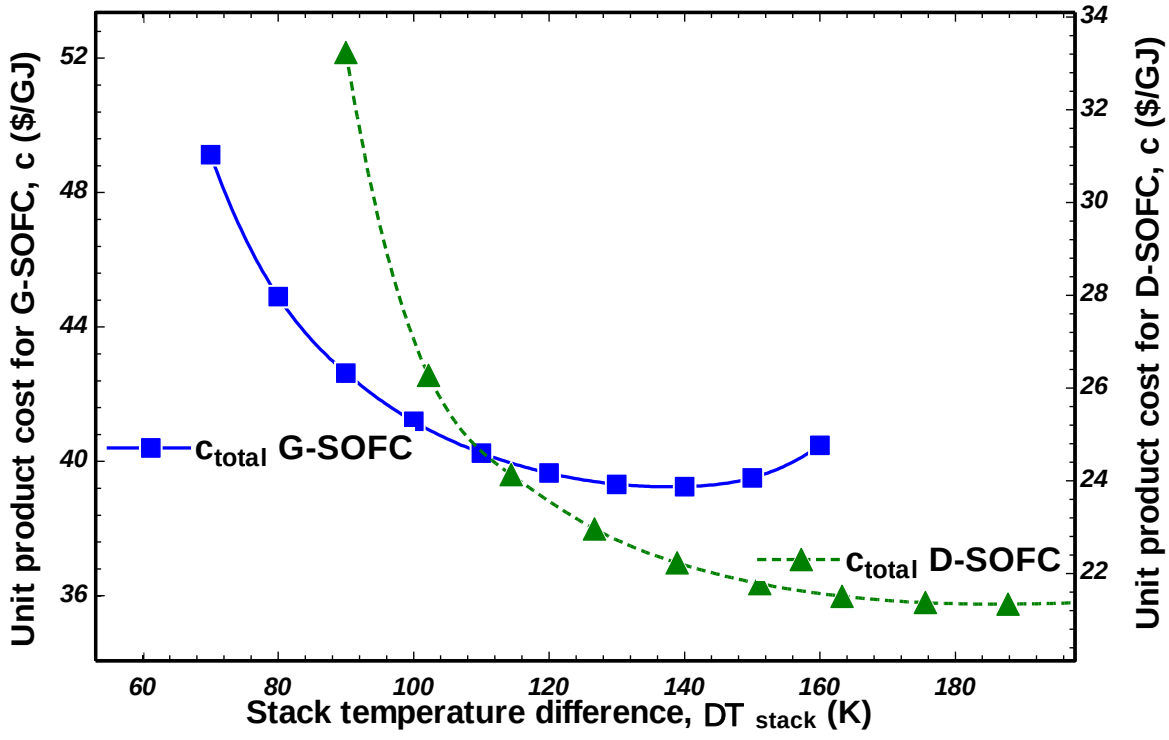

Figure 6 effect of stack temperature difference on a) net power output and heating capacity b) unit product cost of heating and power c) total product cost of digester coupled SOFC and gasifier coupled SOFC

898

a)

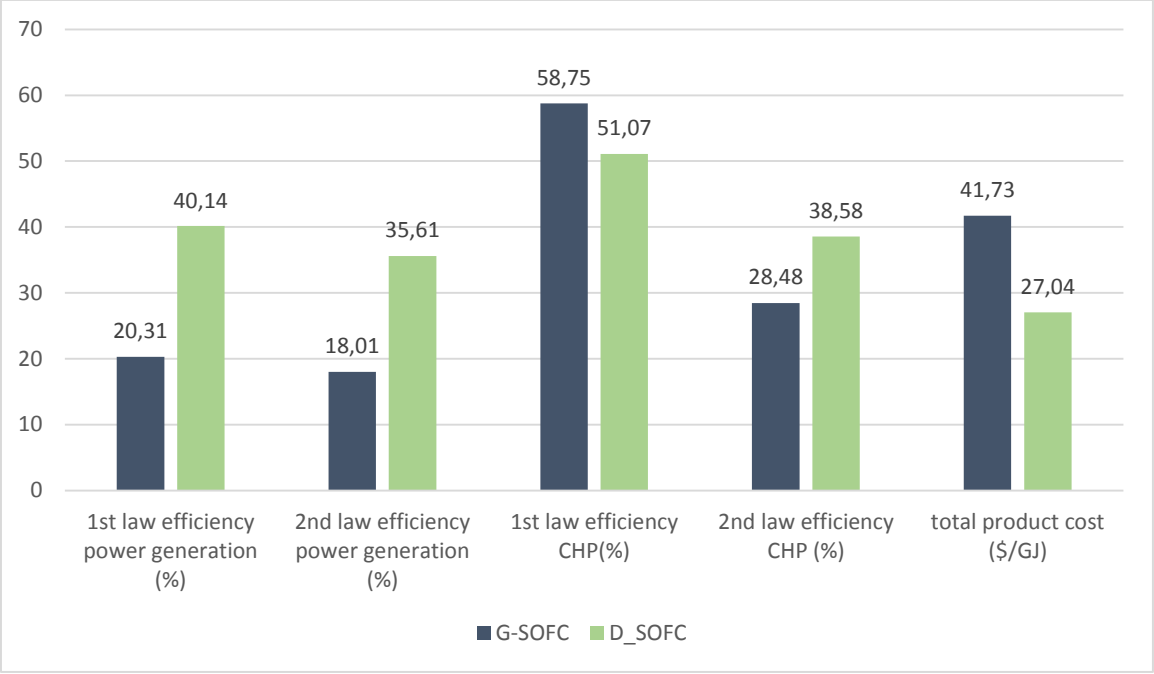

b)

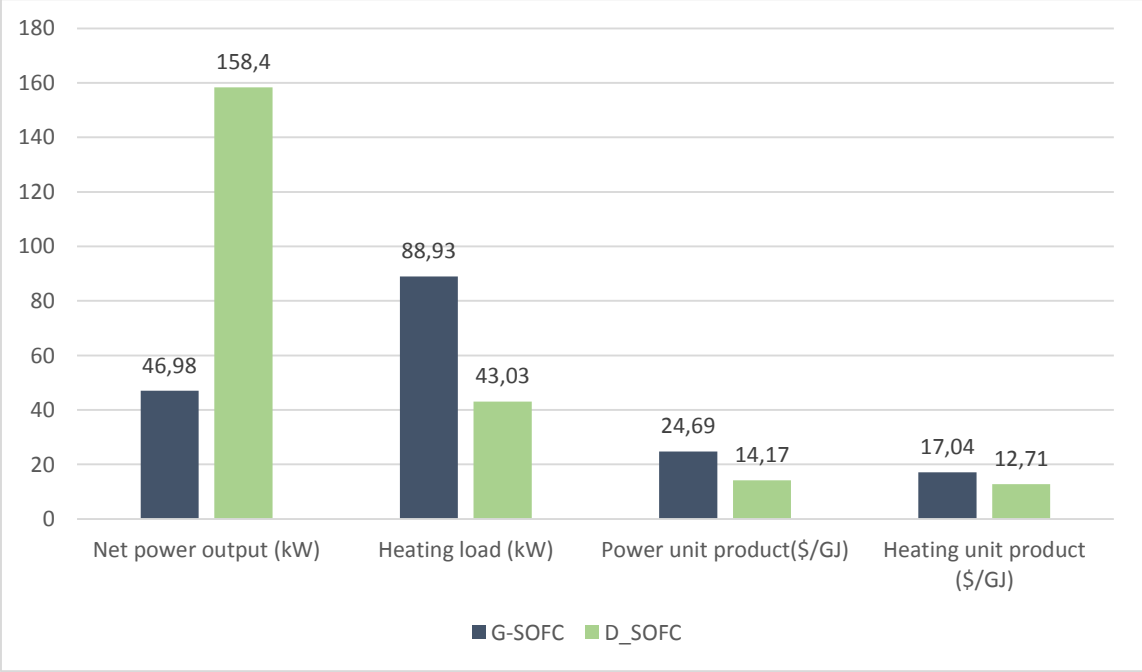

Figure 7 Comparison of a) first and second law efficiencies of systems as well as the total product cost b) net output power and heating load of systems as well as the their product costs

899

a)

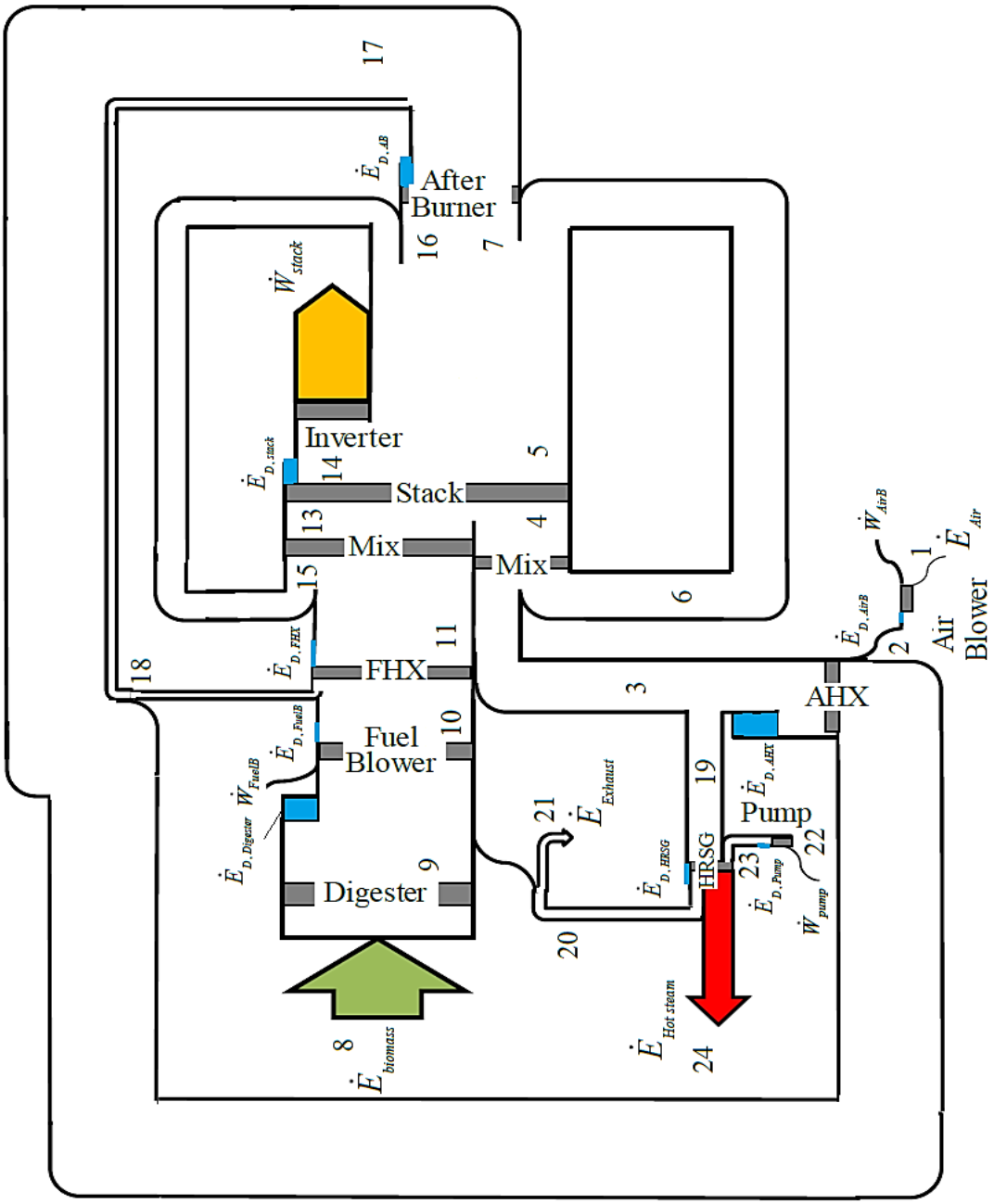

17
After
Burner
16
7
Inverter
14
Stack
5
13
Mix
4
Mix
15
6
11
FHX
18
3
AHX
Fuel
Blower
10
19
Pump
21
22
23
HRSG
9
Digester
20
8
24
1
2
Air
Blower

b)

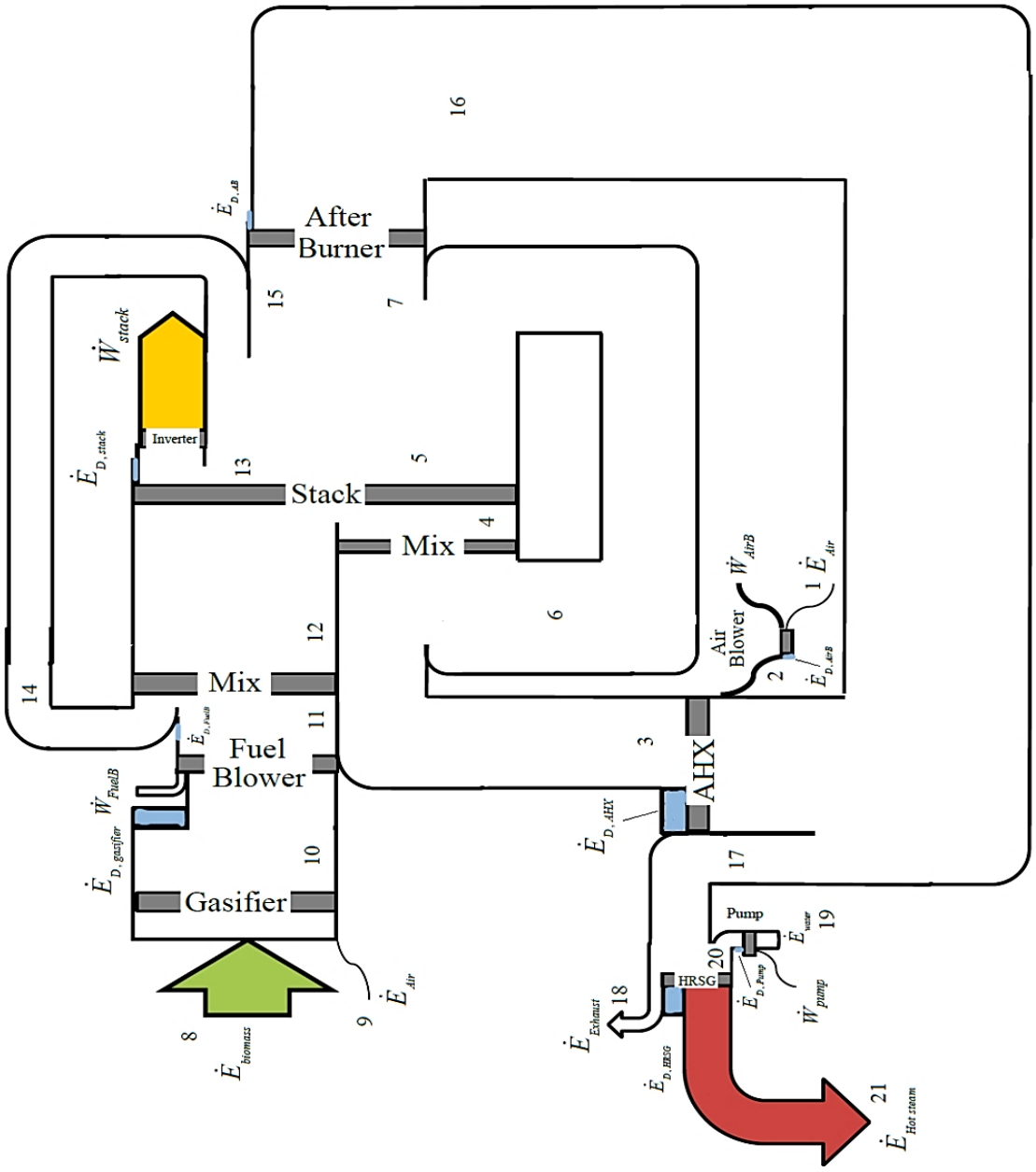

Figure 8 Grassman diagram of the a) digester coupled CHP system based on SOFC (D-SOFC) b) gasifier coupled CHP system based on SOFC (G-SOFC)

900

901

902

903 # Tables

Table 1. Input data for the SOFC systems [34,37,45,55]

SOFC system			**Unit**
	Temperature difference between stack inlet and outlet	100	K
	Fuel utilization factor for whole SOFC	0.80	-
	Active surface area	50	cm^2
	DC-AC inverter efficiency	97	%
	Base inlet temperature to SOFC	973.15	K
	Steam to carbon ratio	2	-
	Thickness of anode	500	μm
	Thickness of cathode	50	μm
	Thickness of electrolyte	10	μm
	Fuel blower isentropic efficiency	80	%
	Air blower isentropic efficiency	80	%
	Pump isentropic efficiency	80	%
	Number of cells	11,000	-
	Afterburner combustion efficiency	99	%
	Stack pressure drop	2	%
	Heat exchangers pressure drop	3	%
	Afterburner pressure drop	5	%
Digester			
	Work needed to drive the fan	0	kW
	Exit temperature (Thermophilic digester)	328	K
	Amount of volatile solid	95	%
	Amount of destruction in digester	70	%
Gasifier			
	Gasification temperature	1073.15	K
	Heat loss from gasifier	0	%
	Air inlet temperature	298	K
	Biomass inlet temperature	298	K
HRSG			
	Pinch point temperature difference	15	K
	Steam pressure	10	bar
	Water pump isentropic efficiency	0.75	-

904

905

906

907

Table 2 Ultimate analysis of MSW [39]

Biomass	C	H	N	S	O	Ash	Higher heating value (kJ/kmol)
Municipal solid waste	47.6	6	1.2	0.3	32.9	12	433034

908

909

Table 3. The comparison of the component percentages in the producer gas obtained from the gasification in the present work and those reported in the literature, for wood with a moisture content of 16% and for a gasification temperature of 1100K.

Constituent	Present model	Experiment [40]	Jarungthammachote equilibrium model [42]
Hydrogen	17.15	15.5	18.04
Carbon monoxide	19.28	19.1	17.86
Methane	0.55	1.1	0.11
Carbon dioxide	10.81	11.4	11.84
Nitrogen	52.21	52.9	52.15

910

911

Table 4. Comparison of results obtained from the present work with the experimental values reported by Tao et al. [43]

Current density (A/m^2)	Cell voltage (V) (Present work)	Cell voltage (V) (Tao et al.)	Error (%)	Power density (W/m^2) (Present work)	Power density (W/m^2) (Tao et al.)	Error (%)
2000	0.742	0.76	-2.368	0.148	0.15	-1.333
3000	0.684	0.68	0.588	0.205	0.21	-2.381
4000	0.634	0.62	2.258	0.253	0.26	-2.692
5000	0.582	0.57	2.105	0.294	0.295	-0.339
6000	0.547	0.52	5.192	0.328	0.315	4.127

912

913

914

915

916

917

Table 5 Input data* and cost and auxiliary equations for each component [11,33]

Auxiliary equations	Cost equations	Component
$c_{biomass}=2$	$Z_{gasifier}=1600\left(\dot{m}_{drybiomass}\right)^{0.67}$	Gasifier
$c_{biomass}=2$	$Z_{Digester}=350000\left(\frac{\dot{V}\,T}{21000}\right)^{0.75}$	Digester
$\dot{C}_{14}/\dot{E}_{14}=\dot{C}_{33}/\dot{E}_{33}$	$Z_{SOFC}=A_a\,N_{FC}\left(2.96\,T_{FC,e}-1907\right)$	SOFC stack
$\dot{C}_5/\dot{E}_5=\dot{C}_{33}/\dot{E}_{33}$		
-	$Z_{AB}=\frac{46.08\dot{m}_7}{\left(0.955-\left(P_{17}/P_7\right)\right)}\left(1+e^{(0.018T_{17}-26.4)}\right)$	Afterburner
$c_1=0$	$Z_{AC}=91562\left(\dot{W}_{AC}/455\right)^{0.67}$	Air compressor
$c_{10}=c_F$	$Z_{FC}=91562\left(\dot{W}_{FC}/455\right)^{0.67}$	Fuel compressor
$c_{20}=0$	$Z_{P1}=1785\,f_n\left(\dot{W}_P/1\right)^{0.71}$	Pump
	$f_n=1+\left(0.2/\left(1-\eta_P\right)\right)$	
$\dot{C}_{17}/\dot{E}_{17}=\dot{C}_{18}/\dot{E}_{18}$	$Z_{FHX}=130\left(A_{FHX}/0.093\right)^{0.78}$	FHX
$\dot{C}_{18}/\dot{E}_{18}=\dot{C}_{19}/\dot{E}_{19}$	$Z_{AHX}=390\left(A_{AHX}/0.093\right)^{0.78}$	AHX
$\dot{C}_{19}/\dot{E}_{19}=\dot{C}_{20}/\dot{E}_{20}$	$Z_{HRSG}=6570\left(\left(\dot{Q}_{eco}/\Delta T_{eco}\right)^{0.8}+\left(\dot{Q}_{eva}/\Delta T_{eva}\right)^{0.8}\right)+$	HRSG
	$21276\dot{m}_{steam}+1184.4\left(\dot{m}_{gas}\right)^{1.2}$	
-	$Z_{inv}=100000\left(\dot{W}_{SOFC,DC}/500\right)^{0.7}$	Inverter

* *i_r=0.12 , n=20 years, $\tau=8000\,h$,T=retention time in digester, c_F=2$/GJ (biomass)*

918

919

920

Table 6. Exergy and exergy destruction rates for two proposed SOFC systems

Digester Coupled SOFC		Gasifier Coupled SOFC	
Exergy rate	$\dot{E}X(kW)$	Exergy rate	$\dot{E}X(kW)$
Input exergy	462.6	Input exergy	290.3
Destruction		Destruction	
Digester	41.98	Gasifier	74.42
Air blower	7.018	Air blower	3.591
Fuel blower	0.128	Fuel blower	0.3248
AHX	78.67	AHX1	16.29
FHX	4.716	AHX2	35.3
Stack	42.29	Stack	9.304
AB	30.67	AB	12.95
Mixing unit	2.804	Mixing unit	1.018
HRSG	4.840	HRSG	9.786
Pump	0.049	Pump	0.010
Exergy associated with heating	26.27	Exergy associated with heating	54.29
Exergy associated with power	164.3	Exergy associated with power	49.81
Exergy loss	58.7	Exergy loss	26.93
U_f=0.80 , $Tstack = 800\ °C$			

930

931

Table 7 Exergoeconomic analysis results for the gasifier coupled SOFC (G-SOFC)

Components	$\dot{E}_f$ (kW)	$c_{F,k}$ ($/GJ)	$c_{P,k}$ ($/GJ)	$\dot{C}_{D,k}$ ($/h)	$\dot{C}_{L,k}$ ($/h)	$\dot{Z}_k$ ($/h)	$\dot{C}_{D,k}+\dot{C}_{L,k}+\dot{Z}_k$ ($/h)	f_k (%)
SOFC stack	437	16.8	20.05	0.5627	0	4.430	5.00	88.75
Air heat exchanger 1	15.36	4.751	27.87	0.2142	0	0.022	0.236	9.41
Air heat exchanger2	221.9	21.14	26.52	2.974	0	0.567	3.541	16.02
Air blower	15.62	20.05	34.01	0.2592	0	0.345	0.604	57.15
Fuel blower	6.25	20.05	29.92	0.0234	0	0.187	0.210	88.87
After burner	298.8	20.05	21.14	0.9345	0	0.191	1.126	16.99
Gasifier	260.8	2	3.968	0.5358	0	0.839	1.375	61.04
HRSG	37.06	21.14	33.84	0.7448	2.05	0.502	3.296	15.23
pump	0.0405	20.05	67.06	0.0007	0	0.004	0.005	85.78
U_f=0.80 , $Tstack = 800\ °C$								

932

933

Table 8 Exergoeconomic analysis results for the digester coupled SOFC (D-SOFC)

Components	$\dot{E}_f$ (kW)	$c_{F,k}$ ($/GJ)	$c_{P,k}$ ($/GJ)	$\dot{C}_{D,k}$ ($/h)	$\dot{C}_{L,k}$ ($/h)	$\dot{Z}_k$ ($/h)	$\dot{C}_{D,k}+\dot{C}_{L,k}+\dot{Z}_k$ ($/h)	f_k (%)
SOFC stack	911.8	9.172	11.04	1.397	0	5.834	5.846	76.06
Air heat exchanger	441.8	11.87	15.28	3.361	0	1.130	4.452	24.51
fuel heat exchanger	12.81	11.87	19.44	0.2015	0	0.058	0.220	8.732
Air blower	30.53	11.04	20.73	0.2788	0	0.541	0.820	66.01
Fuel blower	0.753	11.04	33.46	0.0051	0	0.045	0.050	89.88
After burner	561.5	11.04	11.87	1.219	0	0.370	1.589	23.31
digester	444.4	2	2.277	0.3039	0	0.097	0.401	24.22
HRSG	18.04	11.87	25.23	0.2068	2.50	0.428	3.143	13.62
pump	0.014	11.04	64.49	0.0001	0	0.002	0.002	93.11
U_f=0.80 , $Tstack = 800\ °C$								

934

935

936

937

938

939

Table 9. Comparison of the published works results with those of the present work

Research	Plant Type; Plant Scale	Fuel; Process; Gas	Thermodynamic analysis		Economic analysis	Year
			1st law Efficiency (%)	2nd law Efficiency (%)	Unit Product Cost	
Omosun et al. [14]	Cogeneration (Heat and power);200kW_{el}	Biomass; Fluidized bed gasification; Syngas (17%H_2,13%CO,11% CO_2,4%CH_4, 15%H_2O,40%N_2)	Electrical: 22.6% Total: 59.6%	-	2.9k £/kW_e 1.1k £/kW_T	2004
Piroonlerkgul et al. [26]	Mono generation (power); small size (50-60kW)	Biogas (60%CH_4,40%CO_2)	Electrical: 59%	-	-	2008
Farhad et al. [56]	Cogeneration (Heat and power);small size (~1kW_{el})	Biogas (60.8%CH_4,34.8%CO_2, 2.4%N_2,1.2%O_2,0.01% water)	Electrical: 22.6% Total: 59.6%	-	-	2010
Bang-Møller et al. [57]	Cogeneration (Heat and power) Hybrid system; medium size (~300kW)	Wood; two-stage gasification; syngas	Electrical: 58.2% Total: 87.5%	Electrical: 50.4% Total: 53.4%	-	2011
Santarelli et al. [29]	Cogeneration (Heat and power); medium size (scale–up 250kW)	Wheat straw; Two-stage anaerobic digester; biogas (55%CH_4,10%H_2,35% CO_2)	Electrical: 49.2% Total: 75.1%	-	-	2012
El-Emam et al. [58]	Mono generation (power) Hybrid system; Large size (~30MW)	Coal gasification; syngas(10.6%CO_2,51.6 %CO,0.1%CH_4,35.1% H_2,2.6%N_2)	Electrical: 38.1%	Electrical: 27%	-	2012
Wongchanapai et al. [59]	Mono generation (power); small scale (5kW)	Wood; two-stage gasification; Syngas(18.7%H_2,21.87 CO,0.22%CH_4,10.51% CO_2,47.3%N_2)	Electrical: 38.9%	Electrical: 37.4%	-	2012
Campitelli et al. [60]	Mono generation (power); small scale (1-2 kW)	Wood; autothermal gasification; syngas (17.8%H_2,9.4%CO,14 %CO_2,19.8%H_2O,0.1% CH_4)	Electrical: 24.7%	-	-	2013
Arteaga-Pérez et	Cogeneration	Sugar cane/rice husk;	Total:	Total:	-	2013

al. [61]	(Heat and power); medium size (456.5kW)	bubbling fluidized bed gasification; syngas (17.5%H_2O,40.1%N_2, 0.6%O_2,6.5%CH_4, 13.6%CO,12.4%CO_2, 9.3%H_2)	55.48%	32.01%		
Morandin et al. [62]	Cogeneration (Heat and power) Hybrid system; small size (~40kW)	Wood; fluidized bed gasifier/Viking gasifier; syngas	Total:63% (For Viking gasifier case) Total: 58% (For fluidized bed gasifier)	-	15000$/kW (For Viking gasifier case) 8000 $/kW (For fluidized bed gasifier)	2013
Trendewicz and Braun [31]	Cogeneration (Heat and power); small, medium and large sizes (330kW,1530kW,6140kW)	Waste water; anaerobic digestion; biogas (56.6%CH_4, 36.7%CO_2,5.8%H_2O)	Electrical: 51.6% Total: 87.5%	-	3584 $/kW (large size) 3916 $/kW (medium size) 5780 $/kW (small size)	2013
Gandiglio et al.[28]	Trigeneration (Heat, power and Algae production); small scale (2kW_{el})	Waste water; anaerobic digester; biogas (60%CH_4,40%CO_2)	Electrical: 52.56% Total: 85.93%	-	-	2014
Siefert and Litster [33]	Mono generation (power)	Waste water; anerobic digestion; Biogas (45%CH_4,40%CO_2,15 %H_2O)	-	Electrical: 58%	3610 $/kW	2014
Ozcan and Dincer [63]	Trigeneration (Heat. power and cooling); medium size (145.5kW)	ThermoChembubling fluidized bed gasifier; syngas (43.3%H_2, 9.2%CO,28%CO_2,5.6 % H_2O,4.7%CH_4)	Electrical: 42.2% Total: 78.8%	Electrical: 36.5% Total: 50.6%	-	2014
Caliandro et al. [64]	Mono generation (power) Hybrid system; small and medium sizes (103kW and 8000kW)	Wood; fast internally circulating fluidized bed gasifier/circulating fluidized bed gasifier/Viking gasifier; syngas	Electrical: 71% (circulating fluidized bed) Electrical: 68.7% (Viking gasifier)	-	0.3 $/kWh (circulating fluidized bed-medium size) 1.1$/kWh (Viking gasifier-small size)	2014
Jia et al. [22]	Cogeneration (Heat and	Wood; downdraft gasifier; syngas	Electrical: 42.94%	-	-	2015

	power) Hybrid system; small size (~40kW)		Total: 67.59%			
Curletti et al. [65]	Mono generation (power); large size (1MW_{el})	Waste water; anaerobic digestion; biogas	Electrical: 58.85%	-	2.75 M$ Net present value	2015
Mehr et al. [34]	Mono generation (power); medium size (~400kW)	Biogas (50-70%CH_4,30%-50%CO_2)	Electrical: 46.09%	Electrical:43.92%	19.53 $/GJ	2015
Lv et al. [66]	Mono generation (power) Hybrid system; small size (182kW)	Wood; gasification; syngas(4.53%CH_4,23.64%H_2,13.87%CO,17.92%CO_2,40.04%N_2)	Electrical: 60.78%	-	-	2016
Present work	Cogeneration (Heat and power); small size	Municipal solid waste; downdraft gasifier; Syngas	Electrical: 20.31% Total: 58.75%	Electrical: 18.01% Total: 28.48%	24.69$/GJ	-
		Municipal solid waste ;anaerobic digestion; biogas	Electrical: 40.14% Total: 51.07%	Electrical:35.61% Total: 38.58%	14.17$/GJ	-

Table A.1. Material Resistivity used for ohmic voltage loss estimation [52]

Component	Material	Resistivity	Thickness (mm)
Anode	Ni/YSZ cermet	$\rho_{an}=2.98\times10^{-5}\exp(\frac{-1392}{T_{FC,e}})$	0.5
Cathode	LSM-YSZ	$\rho_{cat}=8.114\exp(\frac{600}{T_{FC,e}})$	0.05
Electrolyte	YSZ	$\rho_{ely}=2.94\times10^{-5}\exp(\frac{10350}{T_{FC,e}})$	0.01
Interconnection	Doped LaCrO3	0.0003215	-

Table A.2. Parameters correspond to anode and cathode sides material [52]

Component	Parameter	Value	Unit
Anode	Pre-exponential factor for anode, γ_{an}	6.54×10^{11}	A/m^2
	Activation energy for anode, $E_{a,an}$	140,000	J/mol
Cathode	Pre-exponential factor for cathode, γ_{ca}	2.35×10^{11}	A/m^2
	Activation energy for cathode, $E_{a,cat}$	137,000	J/mol